AWARD NUMBER: W81XWH-19-1-0265

TITLE: Overcoming Anti-PD-1 Resistance in Lung Cancer

PRINCIPAL INVESTIGATOR: Nejat Egilmez

CONTRACTING ORGANIZATION: University of Louisville, Louisville, KY

REPORT DATE: November 2022

TYPE OF REPORT: FINAL

PREPARED FOR: U.S. Army Medical Research and Development Command
Fort Detrick, Maryland 21702-5012

REPORT DOCUMENTATION PAGE

Form Approved
OMB No. 0704-0188

1. REPORT DATE	2. REPORT TYPE	3. DATES COVERED
November 2022	Final	01Aug2019-31Jul2022

4. TITLE AND SUBTITLE

Overcoming Anti-PD-1 Resistance in Lung Cancer

5a. CONTRACT NUMBER
W81XWH-19-1-0265

5b. GRANT NUMBER
LC180086

5c. PROGRAM ELEMENT NUMBER

6. AUTHOR(S)
Nejat Egilmez

E-Mail:nejat.egilmez@louisville.edu

5d. PROJECT NUMBER

5e. TASK NUMBER

5f. WORK UNIT NUMBER

7. PERFORMING ORGANIZATION NAME(S) AND ADDRESS(ES)

University of Louisville
2301 S 3rd Street
Louisville, KY 40206

8. PERFORMING ORGANIZATION REPORT NUMBER

9. SPONSORING / MONITORING AGENCY NAME(S) AND ADDRESS(ES)

U.S. Army Medical Research and Development Command
Fort Detrick, Maryland 21702-5012

10. SPONSOR/MONITOR'S ACRONYM(S)

11. SPONSOR/MONITOR'S REPORT NUMBER(S)

12. DISTRIBUTION / AVAILABILITY STATEMENT

Approved for Public Release; Distribution Unlimited

13. SUPPLEMENTARY NOTES

14. ABSTRACT

The goal of this proposal was to first define the cellular and molecular effector mechanisms that underlie our original observation, i.e. lung Th17 immunity drives anti-PD-1 resistance in lung cancer (Aim 1); and then determine whether the lung microbiota signature ultimately determines the severity of Th17 cell activity (Aim 2). All Aim 1 studies and part of Aim 2 subtask 1 were completed in years 1 and 2 along with a publication (see Appendix). Year 3 work saw the completion of Aim 2, subtasks 1 & 2, and the publication of a second manuscript (see Appendix). This concludes all proposed studies.

15. SUBJECT TERMS

Lung cancer, Anti-PD-1, IL-17, Th17 cells, microbiota

16. SECURITY CLASSIFICATION OF:			17. LIMITATION OF ABSTRACT	18. NUMBER OF PAGES	19a. NAME OF RESPONSIBLE PERSON
a. REPORT	b. ABSTRACT	c. THIS PAGE			19b. TELEPHONE NUMBER *(include area code)*
Unclassified	Unclassified	Unclassified	Unclassified	35	USAMRDC

Standard Form 298 (Rev. 8-98)
Prescribed by ANSI Std. Z39.18

TABLE OF CONTENTS

INTRODUCTION

This is the final report for the above grant. We have completed all proposed tasks and have published our results in two companion papers (Appendix).

KEYWORDS

Lung cancer, anti-PD-1, IL-17, Th17 cells, microbiota.

ACCOMPLISHMENTS

***Specific Aim 1*. To define the cellular and molecular effector mechanisms that mediate anti-PD-1-Th17 cell axis-driven therapeutic resistance in the LSL-K-ras^{G12D} lung cancer model (Months 1-18)**.

All tasks were completed and published in two back-to-back articles (Appendix).

Major Task 1. To confirm the effect of anti-PD-1 on lung-associated Th17 cells in the LSLKras spontaneous lung cancer model.

Subtask 1. Obtain ACURO approval (Months 1-3). ACURO approval was obtained.

Subtask 2. Is anti-PD-1-mediated enhancement of Th17 effector activity solely responsible for ICI resistance? (Months 3-9). First, tumor growth / anti-PD-1 resistance was analyzed in mice that were depleted of either CD4+ or γδT-cells. The data showed that CD4+ T-cells contributed to tumor growth only in the presence of anti-PD-1. In contrast, γδT-cells contributed to tumor growth equally in the absence or presence of anti-PD-1 treatment (Figures 1 and 3, Li Q et al Cancer Immunol Immunother epub 2020, Appendix). These data suggested that the CD4+ T-cell component was critical to resistance to anti-PD-1. To this end, tumor growth / anti-PD-1 resistance was analyzed in a more targeted study in which the effect of anti-PD-1 on tumor growth was determined in CD4+ T-cell-specific RORc (transcription factor that drives IL-17 expression) knockout bone marrow chimeras. The results established that Th17 cells were the major mediators of the anti-PD-1-IL-17 axis ((Figure 1, Li Q et al, Cancer Immunol Immunother, epub 2022, Appendix). Additional studies demonstrated that CD4+ T-cell-produced IL-17 mediated its detrimental effects via abrogation of the anti-PD-1-CD8+ T-cell axis (Figures 2 and 3B, Li Q et al Cancer Immunol Immunother epub 2020, Appendix).

Subtask 3. Does Th17/CTL functional balance correlate with therapeutic efficacy? (Months 9-11) In the mouse model, therapeutic outcome correlated with post-treatment Th17 cell prevalence alone (Figure 3C, Li, Q et al., epub 2020, Appendix). In patients, the pre-treatment ratio of CD8+ T-cells to RORc+ cells correlated best with favorable outcome (Table 1 and Figure 4, Li, Q et al., epub 2020, Appendix).

Subtask 4. How does anti-PD-1-Th17 axis counteract anti-PD-1-CTL axis? (Months 11-18) Myeloid-derived Suppressor Cell (MDSC) prevalence or activity did not correlate with the ability of IL-17 to suppress CD8+ T-cell cytotoxicity (Figure 3A, Li Q et al, Cancer Immunol Immunother, epub 2022, Appendix). However, IL-17-driven induction of the enzyme COX-2 and its downstream metabolite PGE2 in macrophages and monocytes was found to mediate the ability of IL-17 to block CD8+ T-cell re-invigoration by anti-PD-1 (Figure 3B-G, Li Q et al, Cancer Immunol Immunother, epub 2022, Appendix). Since COX-2/PGE2 axis fully accounted for the observed suppression, other potential mechanisms that were proposed in the original application were not pursued.

***Specific Aim 2*. To delineate the role of lung microbiota in the ontogeny of tumor-elicited Th17 immunity and resistance to ICI therapy (Months 15-24)**.

Major Task 2. Determine the role of lung microbiota in Th17 ontogeny and anti-PD-1 resistance.

Subtask 1. Are lung commensals the primary drivers of Th17 cell ontogeny and ICI resistance in the dysplastic lung? (Months 15-20). Depletion of lung microbiota resulted in a reduction in tumor burden, which diminished further in a statistically significant manner upon treatment with anti-PD-1 (Li Q et al, Cancer Immunol Immunother, epub 2022, Figure 2A and E, Appendix). We further determined the effect of intratracheal antibiotics on lung resident Th17 cell as well as CTL activity in control and treatment groups. The results showed that depletion of lung bacteria diminished all CD4+ T-cell subsets, but particularly the Th17 subset (Li Q et al, Cancer Immunol Immunother, epub 2022, Figure 2B/C, appendix). In contrast, elimination of bacteria

enhanced CD8+ T-cell cytotoxicity (Li Q et al, Cancer Immunol Immunother, epub 2022, Figure 2B/C, appendix). Analysis of myeloid cell subsets revealed that lung macrophages were responsible for the expansion of Th17 cells in microbiota-sufficient (but not in microbiota-deficient) lungs; and that the phenotype/function of these macrophages were driven by the lung microbiota (Li Q et al, Cancer Immunol Immunother, epub 2022, Figure 2D, appendix).

Subtask 2. Does bacterial signature determine the severity of Th17 cell activity/ICI resistance in individual mice? (Months 20-24). A 16S DNA analysis was partially successful in identifying minor differences between the bacterial signatures of low vs high-tumor burden groups (Figure 1 below). Individual mice did not produce an interpretable pattern. We anticipate this was due to technical challenges associated with processing the ultra-low bacterial yields in individual lungs. These studies were not pursued further.

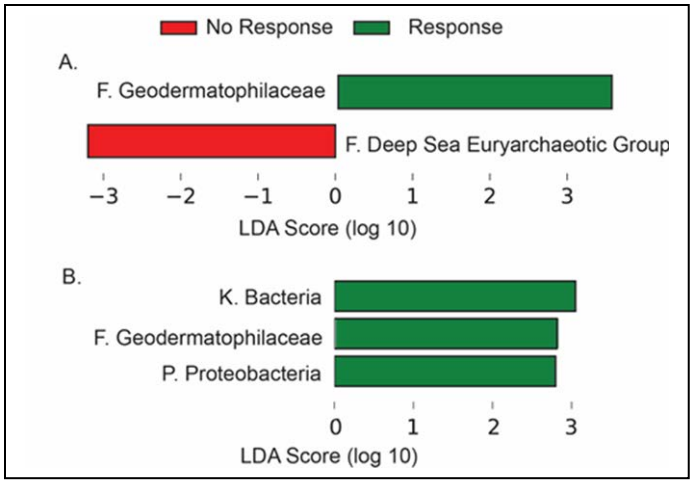

Figure 1. Bacterial signature analysis of lungs in responder vs. non-responder mice. Linear Discriminant Analysis effect size using the Silva classifier (A) and the Greengenes classifier (B) with an alpha of 0.1 and LDA score threshold of 1.5. LSL-Kras mice (6-8wk old) were inoculated with Ad-Cre (2.5 x 10E7 pfu) on day 0. All mice were treated with the combination of anti-PD-1 (1 ug) via IMIT and anti-IL-17A mAb (100 ug) via ip injection twice per week starting on week 7 for 3 wks. Left lung tissue was stained with hematoxylin and eosin (H&E) and the images of lung tissues were taken with the Panoramic Desk DW II. The tumor burden was defined as the ratio of hyperplastic lesion area in each slide to total lung section area. Qupath software was used to analyze digital lung lesions. The right lung was used to isolate gDNA with Qiagen DNeasy blood & tissue kit. 16s rRNA sequencing was carried out in UofL Sequencing Technology Center. Mice with low (<25%) lung tumor burden were classified as responders, mice with high tumor burden (>35%) were classified as non-responder (n= 6 and 5, respectively).

IMPACT

We have demonstrated in two back-to-back publications that: 1) Anti-PD-1 antibody-mediated activation of type 17 T-cells undermines checkpoint inhibitor therapy in the LSL-$Kras^{G12D}$ murine lung cancer model; 2) the Th17 subset is the primary driver of resistance to therapy; 3) the ontogeny of dysplasia-associated Th17 cells is driven by microbiota-conditioned macrophages; and 4) the IL-17-COX-2-PGE_2 axis is the mediator of $CD8^+$ cytotoxic T-lymphocyte de-sensitization to checkpoint inhibitor therapy. These findings have important clinical implications as they not only identify a new paradigm in immune checkpoint blockade resistance, but also reveal the molecular basis of such resistance. Most importantly, our findings offer the possible use of readily available reagents in combination with anti-PD-1 antibody to overcome such resistance in lung cancer patients.

CHANGES/PROBLEMS

No changes were introduced to the original proposal.

PRODUCTS

Li Q, Ngo PT, Egilmez NK. Anti-PD-1 antibody-mediated activation of type 17 T-cells undermines checkpoint blockade therapy. *Cancer Immunol Immunother*. **2020 Nov 27 epub**. Print 2021 Jun;70(6):1789-1796. doi: 10.1007/s00262-020-02795-2. PMID: 33245376.

Li Q, Goggin KE, Seo S, Warawa JM, Egilmez NK. Anti-PD-1 antibody-activated Th17 cells subvert re-invigoration of antitumor cytotoxic T-lymphocytes via myeloid cell-derived COX-2/PGE_2. *Cancer Immunol Immunother*. **2022 Sep 8 epub**, doi: 10.1007/s00262-022-03285-3. PMID: 36074159.

PARTICIPANTS & OTHER COLLABORATING ORGANIZATIONS

There were no changes to the original proposal. No external collaborators were involved.

SPECIAL REPORTING REQUIREMENTS

N/A

APPENDICES

1. Award Expiration Transition Plan.

2. Li Q, Ngo PT, Egilmez NK. Anti-PD-1 antibody-mediated activation of type 17 T-cells undermines checkpoint blockade therapy. *Cancer Immunol Immunother*. **2020 Nov 27 epub**. Print 2021 Jun;70(6):1789-1796. doi: 10.1007/s00262-020-02795-2. PMID: 33245376.

3. Li Q, Goggin KE, Seo S, Warawa JM, Egilmez NK. Anti-PD-1 antibody-activated Th17 cells subvert re-invigoration of antitumor cytotoxic T-lymphocytes via myeloid cell-derived COX-2/PGE2. *Cancer Immunol Immunother*. **2022 Sep 8 epub**, doi: 10.1007/s00262-022-03285-3. PMID: 36074159.

Transition Plan Questionnaire

Directions: Please answer all questions that apply for each product under development. Please fill out one document per product.
This is not an application for funding; however, answers will help us understand the outcomes and products from your award.

1. After the award closes, would you be willing to periodically provide voluntary information (via email) regarding the project status (i.e. where the research is headed)? **Yes** ☐ or **No** ☑
These responses will help CDMRP demonstrate the return on its investments and will help demonstrate that the CDMRP is a responsible and successful steward of federal research funding.

2. What **conclusion(s)** does your final data support?

Targeting IL-17 during anti-PD-1 therapy may benefit lung cancer patients.

3. Will you/have you applied for/obtained follow-on-funding for this project? **If yes**, please list (a) funding organization, (b) total budget requested/obtained, and (c) title of the funded proposal. *This information will be recorded as an outcome to this award*.

No.

4. What will be **the next step(s)** for this project?

None. I am retiring.

5. How would you classify your **lead candidate product**? a
(a) Therapeutic (Small Molecule, Biologic, Cell/Gene Therapy): Please choose, if applicable
(b) Diagnostic
(c) Device
(d) Research Tool to Address a Research Bottleneck
(e) Knowledge Product (Non-material product such as a compound library, database, something that improves clinical practice, education, etc.)
(f) Other - Please Specify:

6. How does your candidate product aid the Warfighter, Veteran, Beneficiary, and/or General Population?

Veterans/military personnel are high risk smokers with increased probability of developing lung cancer. Our findings will help to enhance treatment outcomes.

7. Therapy / Product Development, Transition Strategies, and Intellectual Property

Describe the steps and relevant strategies required to move the candidate product (knowledge or tangible) to the next phase of development and/or commercialization. Please address any issues with intellectual property.

PIs are encouraged to explore the technical requirements and the current regulatory strategies involved in product development as well as to work with their organization's Technology Transfer Office (or equivalent regulatory/legal office), federal/international regulatory experts, to develop the transition plan and to explore developing relationships with industry, DoD advanced developers (e.g. USAMMDA), and/or other funding agencies to facilitate moving the product into the next phase.

Potential IP disclosed to University of Louisville prior to this award. Existing anti-IL-17 antibodies or COX-2 inhibitors may be used in the clinic in conjunction with anti-PD-1 antibody therapy.

Cancer Immunology, Immunotherapy
https://doi.org/10.1007/s00262-020-02795-2

RESEARCH REPORT

Anti-PD-1 antibody-mediated activation of type 17 T-cells undermines checkpoint blockade therapy

Qingsheng Li[1,3] · Phuong T. Ngo[2,3] · Nejat K. Egilmez[1,3]

Received: 25 September 2020 / Accepted: 7 November 2020

Abstract

Tumors that develop in the genetic LSL-K-ras^{G12D} murine lung cancer model are resistant to anti-PD-1 antibody treatment. Analysis of tumor-bearing lungs from anti-PD-1-treated mice revealed an up to 2.5-fold increase in IL-17-producing T-cells, with minimal change in CD8$^+$ T-cell activity. Neutralization of IL-17 concurrent with anti-PD-1 treatment on the other hand, resulted in robust CD8$^+$ T-cell activation and a threefold reduction in tumor burden. Loss-of-function studies demonstrated that anti-PD-1 driven activation of CD4$^+$ and γδTCR$^+$ T-cells contributed to IL-17-mediated de-sensitization of CD8$^+$ cytotoxic T-cells (CTL) to therapy; and that CTL activation was critical to tumor eradication. Importantly, post-therapy lung Th17 cell prevalence and activity prognosticated treatment efficacy. Consistent with the murine data, analysis of tumor biopsy samples from non-small cell lung cancer (NSCLC) patients revealed that pre-therapy intratumoral CD8$^+$/RORc$^+$ cell ratio correlated with response to immune checkpoint blockade (ICB). These findings provide the initial evidence for a new mechanism of ICB resistance in lung cancer.

Keywords Anti-PD-1 · NSCLC · IL-17 · Checkpoint blockade resistance · CD4 T-cell · Th17 cell

Introduction

Immune checkpoint inhibitors, in particular anti-PD-1 antibodies, represent a new paradigm in the management of NSCLC [1]. At the same time, while effective in a subset of patients as first or second line therapy, anti-PD-1 still fails in 50–75% of NSCLC patients [1]. High tumor PD-L1 expression and neoantigen burden correlate with anti-PD-1 responsiveness, and in part may explain the suboptimal response rates [1, 2]. However, 30–40% of PD-L1-positive and high neoantigen burden tumors still do not respond while up to 14% of low neoantigen tumors do respond [3] suggesting that other, yet unidentified, factors contribute to resistance. To this end, the broader tumor immune signature, the functional ontogeny of tumor-infiltrating CD8$^+$ T-cells as well as the commensal microbiota have been identified as other contributors to responsiveness, but are yet to provide specific measurable prognostic markers in the clinical setting [2].

To gain further insight into this conundrum we investigated the therapeutic potential of anti-PD-1 antibody in the checkpoint blockade-resistant, low-neoantigen burden LSL-K-ras^{G12D} murine spontaneous lung cancer model [4–6]. Anti-PD-1 antibody had no detectable therapeutic benefit in LSL-K-ras^{G12D} mice, confirming previous findings [6]. Phenotypic and functional analyses of lung T-cell populations revealed that anti-PD-1-mediated activation of lung-intrinsic Type 17 T-cells (T17 cells) directly interfered with the ability of the antibody to activate antitumor CD8$^+$ T-cells, and that post-therapy lung Th17 cell prevalence was predictive of therapeutic outcome in individual mice. Consistent with these findings, preliminary analysis of NSCLC patient tumor biopsies revealed a correlation between intratumoral CD8$^+$/RORc$^+$ cell ratio and tumor responsiveness to ICB. This is

Electronic supplementary material The online version of this article (https://doi.org/10.1007/s00262-020-02795-2) contains supplementary material, which is available to authorized users.

✉ Qingsheng Li
qingsheng.li@louisville.edu

✉ Nejat K. Egilmez
nejat.egilmez@louisville.edu

[1] Department of Microbiology and Immunology, School of Medicine, University of Louisville, 505 S. Hancock St., Louisville, KY 40202, USA

[2] Department of Medicine, School of Medicine, University of Louisville, Louisville, KY 40202, USA

[3] James Graham Brown Cancer Center, University of Louisville, Louisville, KY 40202, USA

Published online: 27 November 2020

the first report of a potential role for anti-PD1-mediated T17 cell activation in resistance to ICB.

Materials and methods

Mice and tumor model

LSL-K-ras^{G12D} (B6.129S4-Krastm4Tyj/J) mice were purchased from The Jackson Laboratory (Bar Harbor, ME). Tumors were induced as described previously [7]. All experiments were approved by the University IACUC.

Patient samples

De-identified NSCLC patient tumor biopsy specimens were obtained from the Brown Cancer Center Biorepository, University of Louisville. Tissue sections prepared from formalin-fixed, paraffin-embedded tumor samples were processed for RNAscope. The study was approved by the University Institutional Review Board.

Microsphere preparation and treatment

Anti-PD-1 antibody-encapsulated biodegradable polylactic acid microspheres were prepared as previously described [7]. Two formulations were produced: (1) control (no antibody) and (2) anti-mouse CD279 (PD-1) antibody (clone J43, BioXCell, West Lebanon, NH) with a loading of 8 µg antibody/mg of particles. Control or anti-PD-1 microspheres (0.125 mg particles in 35 µl sterile water) were administered via intubation-mediated intratracheal instillation (IMIT) 2x/week for 4 weeks starting 6 weeks after adenoviral infection [7]. Soluble antibody (200 µg in 0.2 ml saline) was administered i.p. 3x/week.

In vivo antibody-mediated leukocyte subset depletion and cytokine neutralization

Depletion was performed by i.p. injection of 250 µg of anti-mouse CD4 (clone GK1.5), CD8 (clone 53-6.72, BioXCell) or via i.v. injection of γδTCR antibody (clone UC7-13D5, BioXCell or Leinco Technologies) 3x/week for 4 weeks. For in vivo neutralization of IL-17, 100 µg anti-mouse IL-17A (clone 17F3; BioXCell) was administered i.p. 3x/week for 4 weeks.

Tumor quantification

Lung tumor burden was quantified by digital imaging analysis of H&E-stained serial lung sections as described previously [7]. QuPath open source software was used to quantify lesion vs total lung area per section.

Isolation of lung mononuclear cells

Lung mononuclear cells were isolated as previously described [7].

Antibodies and flow cytometry

Fluorescence-conjugated anti-CD4 (RM4-5), anti-CD8a (53-6.7), anti-γδTCR (GL3), anti-CD11b (M1/70), anti-Gr-1 (RB6-8C5), anti-Ly-6G (1A8), anti-IL-17A (TC11-18H10.1), anti-IFN-γ (XMG1.2) and anti-RORγt (Q31-378), were purchased from BioLegend (San Diego, CA), eBioscience (Waltham, MA) or BD Biosciences (San Jose, CA). Foxp3 (PJK-16s; eBioscience) was quantified by intracellular staining performed according to the manufacturer's protocol. For intracellular cytokines, cells were stimulated for 4 h with PMA and ionomycin (Sigma-Aldrich, St. Louis, MO) in the presence of brefeldin A (Sigma-Aldrich) and stained with antibodies. For CD107a degranulation assay, cells were cultured in RPMI1640 with anti-CD3 (10 µg/ml) and anti-CD28 (1 µg/ml) in 96-well plates for 24 h; were washed and re-stimulated with PMA and ionomycin in the presence of anti-CD107a (1D4B, BioLegend) for an additional 4 h.

Single-molecule RNA in situ hybridization

RNAscope [8] was performed at Advanced Cell Diagnostics (Newark, CA). Briefly, manual chromogenic staining was performed with paired double-Z oligonucleotide probes for CD8a green (cat. no. 560391) and RORc red (cat. no. 556991) using RNAscope® 2.5 HD Duplex Reagent Kit (cat. no. 322430) per manufacturer's instructions. Each sample was quality controlled for RNA integrity with a probe specific to peptidylpropyl isomerase B. Negative control background staining was evaluated using a probe specific to the bacterial dapB gene. Stained slides were scanned with Aperio ScanScope slide scanner at 40 × objective resolution (Aperio Technologies, Vista, CA). High-resolution images taken with ObjectiveView (Digital Pathology Image Viewer) and TIFF images were then subjected to computerized analysis with Fuji software to quantify positive cells per field.

Statistical analysis

Student's *t* test was used to determine the significance of the differences between control and experimental groups in pairwise comparisons. In experiments with multiple groups, homogeneity of intergroup variance was analyzed by one-way ANOVA with multiple pairwise comparisons

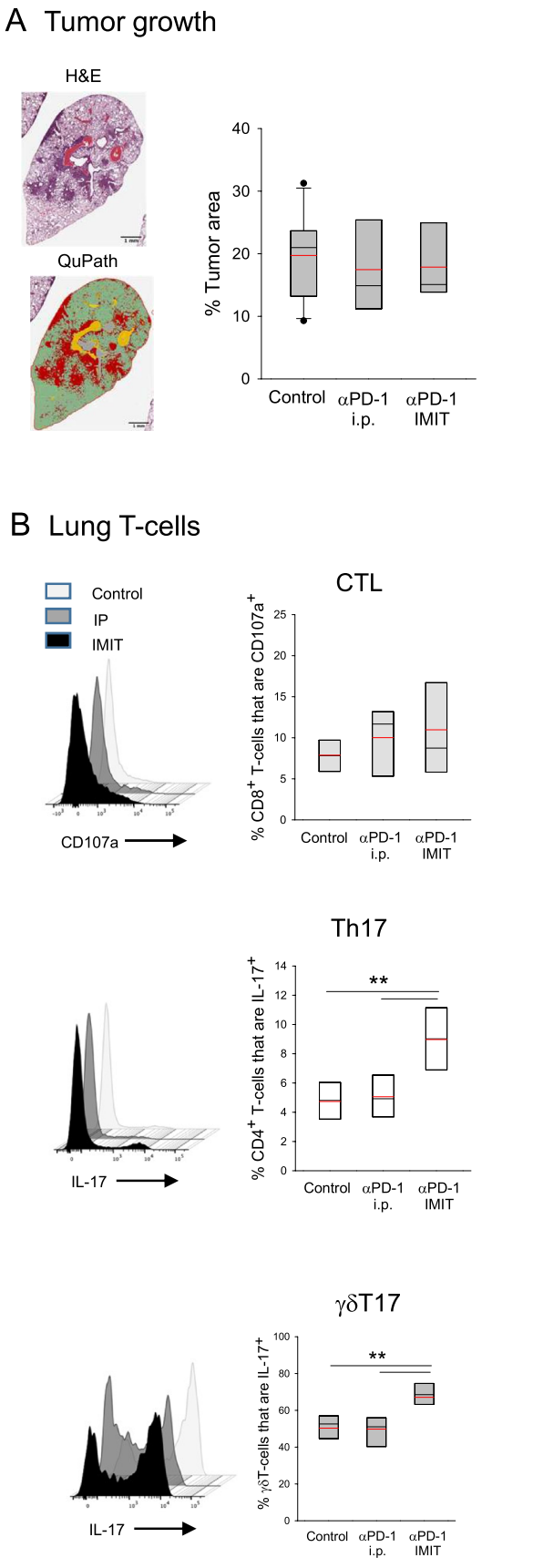

Fig. 1 Effect of anti-PD-1 treatment on tumor growth and lung T-lymphocyte activity. **a** Tumor burden. Tumor-bearing mice were treated with soluble (i.p) or encapsulated (*IMIT* intubation-mediated intratracheal instillation) anti-PD-1 and lungs were analyzed for tumor burden. Representative lung histology (left upper) with accompanying QuPath analysis identifying tumor areas (left lower, in red) and quantitative data (right) are shown. There were no significant differences between the groups ($n=8$–10 per group). **b** T-cell activity. Single cell suspensions prepared from the lungs were analyzed for cytotoxic $CD8^+$ T-lymphocytes ($CD8^+CD107a^+$), Th17 cells ($CD4^+ROR\gamma t^+IL\text{-}17^+$) and γδT17 cells ($\gamma\delta TCR^+ROR\gamma t^+IL\text{-}17^+$). Representative flow cytometry panels and quantitative data are shown ($n=5$ per group). Boxes have lines at the median (black) and mean (red) showing lower (25%) and upper (75%) quartiles. Whiskers extend to show the 10th and 90th percentiles with symbols representing the extreme values (in groups with $n\geq 9$). Significance: asterisks (**) denotes $p<0.01$ (one-way ANOVA with pairwise multiple comparisons, Holm–Sidak)

using Tukey or Holm–Sidak analyses. A p value of <0.05 was considered significant.

Results

Failure of anti-PD-1 therapy is associated with exacerbation of T17 cell activity

We previously demonstrated that intratracheal (i.t.) delivery of a sustained-release IL-10 formulation, but not systemic bolus cytokine, suppressed lung tumorigenesis in the LSL-K-ras^{G12D} model [7]. To this end, we wanted to determine whether a similar formulation of anti-PD-1 antibody could overcome ICB-resistance in these mice. Animals with established lung adenomas were administered either the slow-release formulation or soluble anti-PD-1 i.t. or intraperitoneally (i.p.), respectively. Analysis of lung tumor burden in post-therapy mice demonstrated that treatment failed with either approach (Fig. 1a). To gain further insight into the observed lack of effect, global analysis of lung immune cell infiltrates was undertaken. Immune phenotyping of lung lymphocytes in treated vs control mice revealed a variable effect on $CD8^+$ T-cell cytotoxicity, which did not reach statistical significance (Fig. 1b). In contrast, we observed significant twofold and 1.3-fold increases in Th17 and γδT17 cell activity, respectively, in mice treated with i.t., but not i.p., antibody (Fig. 1b). A minor but significant reduction in Th1 cells was also observed in mice receiving encapsulated antibody while no changes were detected in the prevalence of Treg or the myeloid cell subsets (Supplementary Fig. 1).

Neutralization of IL-17 sensitizes LSL-K-ras^{G12D} lung tumors to anti-PD-1 therapy

Next, we wanted to determine whether exacerbation of T17 cell immunity interfered with the ability of anti-PD-1

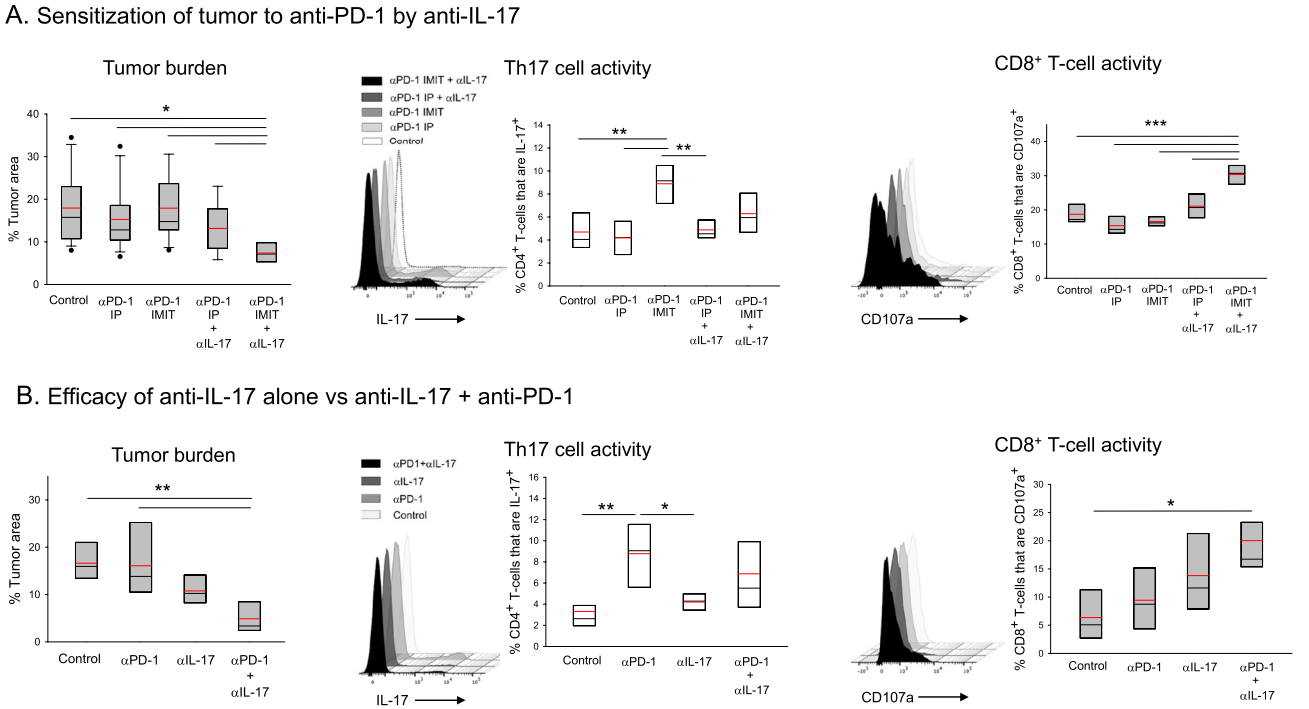

Fig. 2 Effect of IL-17 neutralization on anti-PD-1 therapy. **a** Effect of combined anti-PD-1 + anti-IL-17 antibody treatment on tumor growth and $CD8^+$ T-cell cytotoxicity. Tumor-bearing mice were treated with anti-PD-1 alone i.p (soluble antibody) or via IMIT (slow-release formulation) in the presence or absence of IL-17 neutralization (αIL-17). Tumor burden ($n = 8$–14 per group) and quantitative cellular data for Th17 and $CD8^+CD107a^+$ cells including representative flow cytometry panels are shown ($n = 4$–5 per group). **b** Effect of IL-17 neutralization alone vs anti-PD-1 + anti-IL-17 antibody treatment on tumor growth and $CD8^+$ T-cell cytotoxicity. Mice were treated with control blank microspheres, anti-IL-17 alone (soluble, i.p.), anti-PD-1 alone (encapsulated, via IMIT) or with anti-IL-17 + anti-PD-1. Tumor burden and cellular analysis data are shown ($n = 5$ per group). Significance: asterisks (*, **, ***) denote $p \leq 0.05$, 0.01 and 0.001, respectively (one-way ANOVA with pairwise multiple comparisons, Dunn's or Holm–Sidak)

to stimulate $CD8^+$ T-cell activity. Anti-PD-1 treatment in the presence of IL-17 neutralization resulted in effective tumor suppression in mice that received i.t., but not i.p. anti-PD-1 antibody (Fig. 2a). To gain further insight into the synergy, we examined the post-therapy lung T-cell landscape. Phenotypic analysis of single cell preparations revealed that, in contrast to anti-PD-1 monotherapy, which had no effect on $CD8^+$ T-cells, anti-IL-17 + i.t. anti-PD-1 (but not i.p. anti-PD-1) treatment enhanced $CD8^+$ T-cell membrane CD107a expression by twofold (Fig. 2a); suggestive of an antagonistic relationship between type 17 immunity and CTL reinvigoration.

Since neutralization of IL-17 alone can result in reduced tumor growth in the $LSLKras^{G12D}$ lung cancer model [9], we next determined whether combinatorial treatment was superior to anti-IL-17 alone (using i.t. anti-PD-1 from this point on). Figure 2b data show that while IL-17 blockade alone resulted in a trend towards reduced tumor burden, statistical significance was reached only in the combination group with a > threefold reduction in tumor burden in comparison to controls. Consistent with this finding, analysis of lung T-cell subsets revealed that combination therapy resulted in more effective $CD8^+$ T-cell activation than anti-IL-17 alone.

Th17 and γδT17 subsets contribute to anti-PD-1 resistance via distinct pathways

Next, we investigated the relative roles of Th17 and γδT17 cells in anti-PD-1 resistance. Tumor-bearing mice were treated with anti-PD-1 in the presence or absence of $CD4^+$ or $\gamma\delta TCR^+$ T-cells and tumor burden was analyzed. Administration of anti-PD-1 antibody to $CD4^+$ T-cell-depleted mice resulted in significant tumor suppression in comparison to CD4-sufficient mice (Fig. 3a), while depletion of $CD4^+$ T-cells alone had no effect. We thus concluded that anti-PD-1-mediated activation of $CD4^+$ T-cells played an important role in conferring resistance to therapy. In the case of $\gamma\delta TCR^+$ cell subset however, depletion alone was just as effective as depletion + anti-PD-1 treatment in comparison to anti-PD-1 alone, suggesting that constitutive IL-17 production by γδT-cells contributed to anti-PD-1 resistance (Fig. 3a).

In parallel, analysis of $CD8^+$ T-cells for membrane CD107a in mice that received anti-PD-1 in the absence or

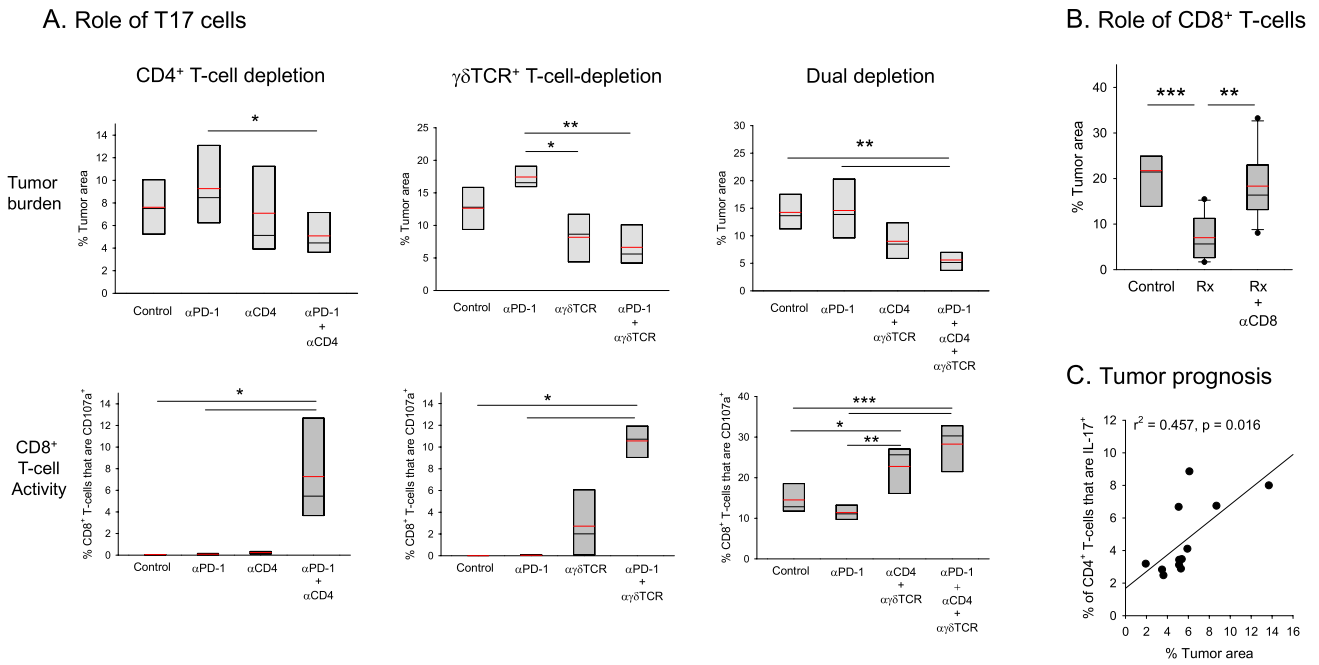

Fig. 3 Roles of T17 cell subsets and CD8$^+$ T-cells in tumor responsiveness and prognosis. **a** Contribution of CD4$^+$ and γδTCR$^+$ cells to anti-PD-1 resistance. The roles of CD4$^+$ T-cells (CD4$^+$ T-cell depletion), γδT-cells (γδTCR$^+$ T-cell depletion), or the two in combination (dual depletion) in resistance to anti-PD-1 were examined. Antibody treatments were as indicated on the abscissa for each plot. Control mice received blank microspheres (via IMIT) without any antibody treatment. Top and bottom panels display the effect of each specific treatment on tumor burden and CD8$^+$ T-cell activity, respectively ($n = 4$–6 per group). **b** Role of CD8$^+$ T-cells in tumor suppression. Mice were treated with anti-PD-1 + anti-IL-17 (denoted as Rx), in the presence or absence of CD8$^+$ T-cell depletion. Control mice received blank microspheres ($n = 8$–13 mice per group). **c** Correlation of Th17 cell prevalence and tumor burden in post-therapy mice. Individual mice were analyzed for tumor burden and Th17 cell prevalence after anti-PD-1 + anti-IL-17 treatment ($n = 12$). Box plots: asterisks (*, **, ***) denote $p \leq 0.05$, 0.01 and 0.001, respectively (one-way ANOVA with pairwise multiple comparisons, Holm–Sidak)

presence of CD4$^+$ T-cells revealed that only the former group displayed significantly increased cytotoxicity (Fig. 3a, lower panels) while CD4$^+$ T-cell depletion alone had no benefit. These data suggested that anti-PD-1-mediated CD4$^+$ T-cell activation interfered with CTL reinvigoration and tumor kill, consistent with the tumor burden data. In the complementary study, analysis of post-therapy CD8$^+$ T-cells in γδT-cell deficient vs sufficient mice indicated that anti-PD-1 induced significant CTL activation in the absence of γδTCR$^+$ cells (Fig. 3a, lower panels). However, unlike what was observed with CD4$^+$ T-cells, depletion of γδT-cells in the absence of anti-PD-1 also resulted in partial CTL activation, again consistent with a role for constitutive IL-17 production by these cells in anti-PD-1 resistance.

Based on these findings, treatment was undertaken in mice with dual depletion of CD4$^+$ and γδTCR$^+$ cells to determine whether this approach would replicate the IL-17-neutralization data. Treatment resulted in a ~ 2.5-fold reduction in tumor burden with a concurrent twofold increase in CD8$^+$ T-cell cytotoxicity in CD4$^+$ and γδTCR$^+$ T-cell depleted mice (Fig. 3a, lower panels) consistent with the IL-17-blockade data. Combined depletion in the absence of treatment was also partially effective suggesting that constitutive IL-17 production, likely by γδT17 cells, maintained CD8$^+$ T-cell suppression at steady-state.

CD8$^+$ T-cells are critical to the ability of anti-PD-1 to induce tumor eradication in the presence of IL-17 neutralization

As the data supported a strong link between CD8$^+$ T-cell activation and tumor suppression, we next performed a loss of function study to directly test this notion. Mice with established disease were treated with anti-IL-17 + anti-PD-1 antibodies in the presence or absence of CD8$^+$ T-cells. Elimination of CD8$^+$ T-cells led to a complete loss of therapeutic efficacy confirming that tumor eradication was strictly dependent on CD8$^+$ T-cells (Fig. 3b).

Post-therapy Th17 cell prevalence is prognostic of treatment outcome in LSLKras^{G12D} mice

Above findings suggested that post-treatment T17 cell prevalence/activity could prognosticate treatment outcome. To this end, mice were analyzed individually for Th17, γδT17 and cytotoxic CD8$^+$ T-cell prevalence and activity as well as

tumor burden following combinatorial therapy. Regression analysis revealed a significant association between post-therapy Th17 cell prevalence and therapeutic outcome (Fig. 3c). In contrast, γδT17 and CTL prevalence, or the functional ratio of CTL to T17 subsets did not correlate with tumor burden (Supplementary Fig. 2a).

Tumor $CD8^+/RORc^+$ cell ratio correlates with checkpoint blockade responsiveness in NSCLC patients

To determine whether we could extend the murine findings to human, pre-treatment lung tumor biopsy samples of NSCLC patients who subsequently received ICB therapy (Table 1), were analyzed for $CD8^+$ and $RORc^+$ cell infiltrates by RNAscope (Fig. 4). Quantitative analysis revealed a statistically significant correlation between the ratio of tumor-infiltrating $CD8^+$ to $RORc^+$ cells and response to therapy. On the other hand, in contrast to the murine model, $RORc^+$ cell prevalence alone was not predictive of ICB responsiveness (Supplementary Fig. 2b).

Discussion

Our data establish that the failure of anti-PD-1 therapy in the LSL-K-ras^{G12D} model is associated with an unexpected exacerbation of lung T17 cell activity that in turn antagonizes $CD8^+$ T-cell reinvigoration. We further demonstrate that Th17 cells are the major responders to anti-PD-1 and that post-treatment Th17 cell prevalence is predictive of therapeutic efficacy in individual mice. Importantly, preliminary analysis of pre-therapy NSCLC patient lung samples revealed a statistically significant correlation between tumor $CD8^+/RORc^+$ cell ratio and subsequent ICB responsiveness, consistent with the murine data. We propose that the intensity of the anti-PD-1-Th17 cell axis may be an important determinant of ICB resistance.

The finding that both $CD4^+$ and $\gamma\delta TCR^+$ T-cells contribute to IL-17-mediated $CD8^+$ T-cell unresponsiveness, but that Th17 cells are the primary prognosticators of outcome for anti-PD-1 treatment is an intriguing observation. Our data suggest that constitutive production of IL-17 by γδT-cells vs anti-PD-1-dependent activation of quiescent Th17 cells may underlie this observation. One caveat is that some of our conclusions regarding the Th17 subset were derived from studies involving total $CD4^+$ T-cell depletion, which cannot exclude potential contribution from T-regulatory cells. However, based on: (a) the identification of IL-17 as the central mediator of anti-PD-1 resistance, and (b) the nearly identical effects of IL-17 blockade and combined $CD4^+ + \gamma\delta TCR^+$ cell depletion on anti-PD-1 efficacy, we expect T-regulatory cells to play a minor role in ICB resistance in this model.

ICB resistance of LSL-K-ras^{G12D} lung tumors [6, 10, 11] has been attributed to low neoantigen burden [5] and suboptimal CTL activity [12]. At the same time, others have reported the presence of significant $CD8^+$ T-cell infiltrates in the tumor-bearing lungs of LSL-K-ras^{G12D} mice [13]. Our findings suggest that these tumors are intrinsically immunogenic and that the $CD8^+$ T-cell infiltrates represent a bona fide antitumor response. Whether the observed CTL response in this model is driven by the G12D mutation [14–16] or involves other epitopes is yet to be determined.

Table 1 Individual data of study patients

Case	Age at diagnosis	Sex	Smoking status	Pathology	Treatment line	ICB	PD-L1 expression (%)	$CD8^+/RORc^+$ cells per field‡	Responder status*	PFS†	Status
1	67	M	Ex-smoker	SCC	First	Pembrolizumab	Unknown	1.75	R	385	Expired
2	63	M	Ex-smoker	AC	First	Pembrolizumab	50	3.18	R	987	Alive
3	74	F	Current smoker	AC	First	Pembrolizumab Atezolizumab	Unknown	1.87	R	420	Expired
4	66	F	Ex-smoker	SCC	First	Pembrolizumab	65	0.98	NR	168	Expired
5	65	M	Ex-smoker	AC	First	Pembrolizumab	0	0.48	NR	42	Expired
6	59	F	Ex-smoker	AC	First	Pembrolizumab	0	0.09	NR	126	Expired
7	61	F	Current smoker	SCC	First	Pembrolizumab	60	0.14	NR	21	Expired
8	62	M	Ex-smoker	SCC	First	Pembrolizumab Nivolumab	0	0.3	NR	126	Expired
9	75	F	Ex-smoker	AC	First	Pembrolizumab	50	0.28	NR	126	Expired

‡Three distinct areas from each section were analyzed and the average numbers of $CD8^+$ and $RORc^+$ cells per representative field (400×) were determined

*Patients that maintained stable disease (SD) for at least 180 days post-treatment initiation were considered responders

†Progression-free survival indicates the time period (days) between first day of treatment and radiological assessment of progression

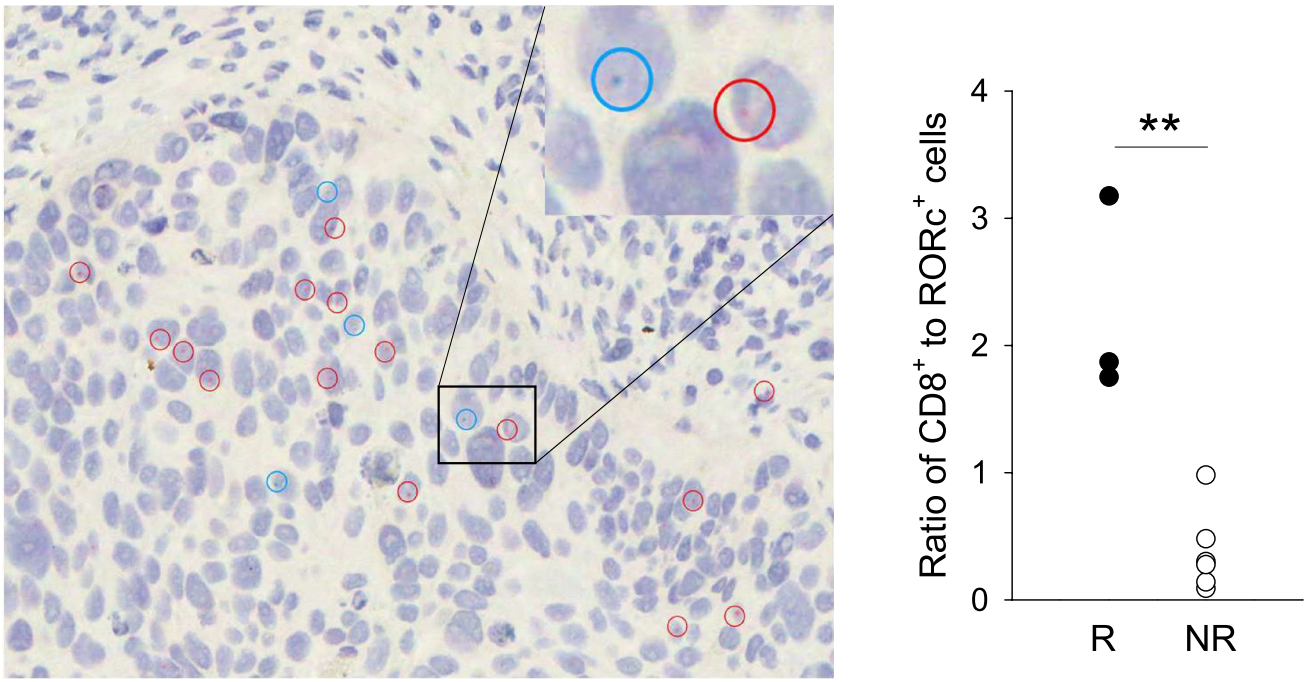

Fig. 4 Analysis of patient tumor $CD8^+$ and $RORc^+$ cell infiltrates. Tissue sections prepared from tumor biopsies were analyzed for CD8a (blue-green) and RORc (red) mRNA by RNAscope. A representative image is shown on the left (magnification = ×400). Cells expressing CD8a or RORc are highlighted with circles of relevant color. Inset displays magnification of the area demarcated by the rectangle. The average ratio of $CD8^+$ to $RORc^+$ cell numbers were calculated for each patient sample and plotted according to response criteria (right panel). The difference between responders (progression free survival > 180 days, $n = 3$) and non-responders ($n = 6$) was significant ($p < 0.01$, Student's t test)

IL-17 is a pleiotropic cytokine that can promote tumor growth directly or indirectly [17]. However, the mechanistic basis of the IL-17-CTL antagonism remains to be elucidated. Potential mechanisms include the IL-17-MDSC axis [18, 19], direct proliferative effects of IL-17 on dysplastic epithelial cells [20], and/or increased PD-L1 expression on epithelium [21].

An intriguing observation that arose from this study was that anti-PD-1 antibody was effective only when delivered locally as a sustained release formulation. A similar observation was previously made with IL-10 [7] suggesting that in this ICB resistant model, i.p. injection may not achieve the therapeutic antibody threshold in the lung, even in the presence of IL-17 blockade. Whether inhalable slow-release formulations represent a more effective alternative to i.v. antibody in individuals that are intrinsically resistant to ICB treatment is to be determined.

The prognostic data obtained in the murine model and the patient samples were conceptually consistent in that type 17 immunity was predictive of response in both. At the same time distinct markers, i.e., post-therapy Th17 cell prevalence in the case of mice and pre-therapy tumor $CD8^+/RORc^+$ cell ratio in patients, associated with responsiveness. Several factors including post- vs. pre-therapy analysis or total lung vs intratumoral assessment of cell populations (in mice vs humans, respectively); patient neoantigen and PD-L1 heterogeneity; and/or the limited patient cohort could all account for the differences observed. Regardless, our findings support a novel role for anti-PD-1-T17 axis in mediating resistance to ICB in lung cancer.

Author contributions NKE: original concept, design and supervision of studies, data interpretation, manuscript preparation, funding. QL: study design, execution of experiments, data interpretation, manuscript preparation. PTN: analysis and interpretation of human data.

Funding This work was supported by the Department of Defense Lung Cancer Research Program Concept award W81XWH1610185 (NKE) and Idea award W81XWH1910265 (NKE).

Data availability All data will be made available upon request.

Compliance with ethical standards

Conflict of interest N.K.E has ownership interest in Therapyx, Inc. The remaining authors declare no competing financial interests.

Ethical approval Murine and human studies were approved by the University of Louisville IACUC and IRB, respectively.

Consent to participate All authors consented to participate in these studies.

Consent for publication All authors consent to publication of the findings.

References

1. Proto C, Ferrara R, Signorelli D et al (2019) Choosing wisely first line immunotherapy in non-small cell lung cancer (NSCLC): what to add and what to leave out. Cancer Treat Rev 75:39–51. https://doi.org/10.1016/j.ctrv.2019.03.004
2. Tunger A, Sommer U, Wehner R et al (2019) The evolving landscape of biomarkers for anti-PD-1 or anti-PD-L1 therapy. J Clin Med. https://doi.org/10.3390/jcm8101534
3. Rizvi NA, Hellmann MD, Snyder A et al (2015) Cancer immunology. Mutational landscape determines sensitivity to PD-1 blockade in non-small cell lung cancer. Science 348:124–128. https://doi.org/10.1126/science.aaa1348
4. Jackson EL, Willis N, Mercer K, Bronson RT, Crowley D, Montoya R, Jacks T, Tuveson DA (2001) Analysis of lung tumor initiation and progression using conditional expression of oncogenic K-ras. Genes Dev 15:3243–3248. https://doi.org/10.1101/gad.943001
5. McFadden DG, Politi K, Bhutkar A et al (2016) Mutational landscape of EGFR-, MYC-, and Kras-driven genetically engineered mouse models of lung adenocarcinoma. Proc Natl Acad Sci USA 113:E6409–E6417. https://doi.org/10.1073/pnas.1613601113
6. Pfirschke C, Engblom C, Rickelt S et al (2016) Immunogenic chemotherapy sensitizes tumors to checkpoint blockade therapy. Immunity 44:343–354. https://doi.org/10.1016/j.immuni.2015.11.024
7. Li Q, Anderson CD, Egilmez NK (2018) Inhaled IL-10 suppresses lung tumorigenesis via abrogation of inflammatory macrophage-Th17 cell axis. J Immunol 201:2842–2850. https://doi.org/10.4049/jimmunol.1800141
8. Wang F, Flanagan J, Su N et al (2012) RNAscope: a novel in situ RNA analysis platform for formalin-fixed, paraffin-embedded tissues. J Mol Diagn 14:22–29. https://doi.org/10.1016/j.jmoldx.2011.08.002
9. Chang SH, Mirabolfathinejad SG, Katta H, Cumpian AM, Gong L, Caetano MS, Moghaddam SJ, Dong C (2014) T helper 17 cells play a critical pathogenic role in lung cancer. Proc Natl Acad Sci USA 111:5664–5669. https://doi.org/10.1073/pnas.1319051111
10. Ritzmann F, Jungnickel C, Vella G et al (2019) IL-17C-mediated innate inflammation decreases the response to PD-1 blockade in a model of Kras-driven lung cancer. Sci Rep 9:10353. https://doi.org/10.1038/s41598-019-46759-8
11. Koyama S, Akbay EA, Li YY et al (2016) Adaptive resistance to therapeutic PD-1 blockade is associated with upregulation of alternative immune checkpoints. Nat Commun 7:10501. https://doi.org/10.1038/ncomms10501
12. DuPage M, Cheung AF, Mazumdar C, Winslow MM, Bronson R, Schmidt LM, Crowley D, Chen J, Jacks T (2011) Endogenous T cell responses to antigens expressed in lung adenocarcinomas delay malignant tumor progression. Cancer Cell 19:72–85. https://doi.org/10.1016/j.ccr.2010.11.011
13. Busch SE, Hanke ML, Kargl J, Metz HE, MacPherson D, Houghton AM (2016) Lung cancer subtypes generate unique immune responses. J Immunol 197:4493–4503. https://doi.org/10.4049/jimmunol.1600576
14. Tran E, Ahmadzadeh M, Lu YC et al (2015) Immunogenicity of somatic mutations in human gastrointestinal cancers. Science 350:1387–1390. https://doi.org/10.1126/science.aad1253
15. Cafri G, Yossef R, Pasetto A et al (2019) Memory T cells targeting oncogenic mutations detected in peripheral blood of epithelial cancer patients. Nat Commun 10:449. https://doi.org/10.1038/s41467-019-08304-z
16. Tran E, Robbins PF, Lu YC et al (2016) T-cell transfer therapy targeting mutant KRAS in cancer. N Engl J Med 375:2255–2262. https://doi.org/10.1056/NEJMoa1609279
17. Kuen DS, Kim BS, Chung Y (2020) IL-17-producing cells in tumor immunity: friends or foes? Immune Netw 20:e6. https://doi.org/10.4110/in.2020.20.e6
18. He D, Li H, Yusuf N, Elmets CA, Li J, Mountz JD, Xu H (2010) IL-17 promotes tumor development through the induction of tumor promoting microenvironments at tumor sites and myeloid-derived suppressor cells. J Immunol 184:2281–2288. https://doi.org/10.4049/jimmunol.0902574
19. Akbay EA, Koyama S, Liu Y et al (2017) Interleukin-17A promotes lung tumor progression through neutrophil attraction to tumor sites and mediating resistance to PD-1 blockade. J Thorac Oncol 12:1268–1279. https://doi.org/10.1016/j.jtho.2017.04.017
20. Wang K, Kim MK, Di Caro G et al (2014) Interleukin-17 receptor a signaling in transformed enterocytes promotes early colorectal tumorigenesis. Immunity 41:1052–1063. https://doi.org/10.1016/j.immuni.2014.11.009
21. Ma YF, Chen C, Li D, Liu M, Lv ZW, Ji Y, Xu J (2017) Targeting of interleukin (IL)-17A inhibits PDL1 expression in tumor cells and induces anticancer immunity in an estrogen receptor-negative murine model of breast cancer. Oncotarget 8:7614–7624. https://doi.org/10.18632/oncotarget.1381919

Cancer Immunology, Immunotherapy
https://doi.org/10.1007/s00262-022-03285-3

BRIEF REPORT

Anti-PD-1 antibody-activated Th17 cells subvert re-invigoration of antitumor cytotoxic T-lymphocytes via myeloid cell-derived COX-2/ PGE_2

Qingsheng Li[1,2] · Kevin E. Goggin[1] · SeonYeong Seo[1] · Jonathan M. Warawa[1,3] · Nejat K. Egilmez[1,2]

Received: 3 May 2022 / Accepted: 22 August 2022

Abstract

Anti-PD-1 antibody-mediated activation of type 17 T-cells undermines checkpoint inhibitor therapy in the LSL-$Kras^{G12D}$ murine lung cancer model. Herein, we establish that the Th17 subset is the primary driver of resistance to therapy demonstrate that the ontogeny of dysplasia-associated Th17 cells is driven by microbiota-conditioned macrophages; and identify the IL-17-COX-2-PGE_2 axis as the mediator of $CD8^+$ cytotoxic T-lymphocyte de-sensitization to checkpoint inhibitor therapy. Specifically, anti-PD-1 treatment of LSL-$Kras^{G12D}$ mice, in which $CD4^+$ T-cells were deficient for RORc, resulted in a 60% increase in CTL cytotoxicity and a 2.5-fold reduction in tumor burden confirming the critical role of Th17 cells in resistance to therapy. Lung-specific depletion of microbiota reduced Th17 cell prevalence and tumor burden by 5- and 2.5-fold, respectively; establishing a link between microbiota and Th17 cell-driven tumorigenesis. Importantly, lung macrophages from microbiota sufficient, but not from microbiota-deficient, mice polarized naïve $CD4^+$ T-cells to a Th17 phenotype, highlighting their role in bridging microbiota and Th17 immunity. Further, treatment with anti-PD-1 enhanced COX-2 and PGE_2 levels, whereas neutralization of IL-17 diminished this effect. In contrast, inhibition of COX-2 rescued CTL activity and restored tumor suppression in anti-PD-1-treated mice, revealing the molecular basis of IL-17-mediated resistance to checkpoint blockade. Clinical implications of these findings are discussed.

Keywords Anti-PD-1 resistance · NSCLC · Th17 cell · Lung microbiota · COX-2 · PGE_2

Introduction

The ability of PD-1-blocking antibodies to achieve effective tumor eradication via re-invigoration of tumor-specific $CD8^+$ cytotoxic T-cells (CTL) is now a well-established paradigm. As a result, immune checkpoint blockade (ICB), either as monotherapy or in combination with cytotoxic agents, has become the standard of care for a variety of cancers including non-small cell lung cancer (NSCLC) [1]. Resistance of tumors to this new modality is generally attributed to tumor-associated factors such as lack of PD-L1 expression and low neoantigen burden, or tumor-extrinsic factors such as the broader immune signature and microbiota [2]. Whether other yet unidentified parameters, intrinsic or extrinsic to the tumor cell, play a role in resistance to ICB remains an active area of investigation.

Whereas the role of anti-PD-1-CTL axis in tumor eradication is well understood, the functional effects of anti-PD-1 antibodies on other immune cell subsets and its implications for ICB are less well described [3]. For example, the literature on how PD-1 blockade alters $CD4^+$ T-cell function in the tumor microenvironment is limited [3], and somewhat controversial in the case of T-regulatory cells [4–7]. In addition, anti-PD-1-mediated activation of different T-helper cell subsets can be beneficial or detrimental to therapeutic outcome depending on the cell type [8, 9].

✉ Qingsheng Li
qingsheng.li@louisville.edu

✉ Nejat K. Egilmez
nejat.egilmez@louisville.edu

[1] Department of Microbiology and Immunology, School of Medicine, University of Louisville, 505 S.Hancock St, Louisville, KY 40202, USA

[2] James Graham Brown Cancer Center, University of Louisville, Louisville, KY 40202, USA

[3] Center for Predictive Medicine, University of Louisville, Louisville, KY 40202, USA

Published online: 08 September 2022

We recently demonstrated that anti-PD-1-mediated activation of Th17, and possibly γδ T17, cells resulted in the abrogation of CTL-mediated tumor killing in the ICB-resistant LSL $Kras^{G12D}$ murine lung cancer model [9]. This finding, combined with extensive murine and human data supporting a pro-tumorigenic role for IL-17 in NSCLC and ICB resistance [10], implicates type 17 T-cell abundance in the tumor microenvironment as a potential driver and prognosticator of resistance to anti-PD-1 [9]. At the same time, while we identified anti-PD-1-T17 cell axis as an important mechanism of resistance to ICB, the specific contributions of individual T17 cell subsets, their ontogeny and how IL-17 mediates CTL de-sensitization to anti-PD-1 in the above model remained undefined. In this follow-up study, we provide further mechanistic insight into these questions.

Materials and methods

Mice. CD45.2 LSL-K-ras^{G12D} (B6.129S4-Krastm4Tyj/J), CD45.1 $Rorc^{fl/fl}$ (B6(Cg)-Rorctm3Litt/J), CD45.1 $CD4^{Cre/+}$ (B6(129X1)-Tg(Cd4-cre/ERT2)11Gnri/J) mice were purchased from the Jackson Laboratory (Bar Harbor, ME) and maintained at University of Louisville. $Rorc^{fl/fl}$ mice were crossed with $CD4^{Cre/+}$ mice to generate $CD4^{Cre/+}/Rorc^{fl/fl}$ mice. For genotyping of $CD4^{Cre/+}/Rorc^{fl/fl}$ mice, the following primers were used: Rorc F 5'-TTC CTT CCT TCT TCT TGA GCA GTC-3'; R 5'-CAG AAG AAA AGT ATA TGT GGC TTG TTG-3'; Generic Cre Transgene F 5'-GCG GTC TGG CAG TAA AAA CTA TC-3'; Transgene R 5'-GTG AAA CAG CAT TGC TGT CAC TT-3'; Internal pos ctl F 5'-CTA GGC CAC AGA ATT GAA AGA TCT-3' Internal pos ctl R 5'-GTA GGT GGA AAT TCT AGC ATC ATC C-3', amplifying Rorc wt (166 bp), CD4-cre transgene (~100 bp), internal positive control (324 bp), and Rorc mutant (226 bp). Mice were housed in a specific pathogen-free facility at the University of Louisville's School of Medicine, and 6 to 10 week-old male and female mice were used in experiments. All experiments were approved by the Institutional Animal Care and Use Committee.

Tumor induction and analysis

To induce tumors, LSL-K-ras^{G12D} mice were anesthetized with isoflurane and then intranasally infected with 2.5×10^7 PFUs of Ad5CMVCre (Ad^{Cre}, Viral Vector Core Facility, University of Iowa) in two 30-µl instillations (administered dropwise to alternating nostrils). Lung tumor burden was quantified by quantitative imaging analysis software (QuPath) of H&E-stained serial lung sections essentially as described by us previously [9]. Tumor burden was defined as the ratio of total hyperplastic areas to total lung area in each section, and all data from a single mouse were averaged to obtain the final percentage of tumor area per animal.

Conditional lineage-specific knock-out bone marrow chimera (BMC) model

BMC were generated by i.v. transfer of T-cell depleted bone marrow cells (1×10^7) derived from $CD4^{Cre/+}/Rorc^{fl/fl}$ mice into lethally irradiated (1,100 rad) LSL-K-ras^{G12D} mice. For tamoxifen-inducible RORc depletion, tamoxifen (Sigma) was dissolved in corn oil at a concentration of 20 mg/ml overnight at 37 °C. The recipient LSL-K-ras^{G12D} mice were given tamoxifen (100 µl) via intraperitoneal (i.p.) injection once every 24 h for a total of 5 consecutive days as indicated.

Anti-PD-1 microspheres and treatment

Anti-PD-1 antibody-encapsulated biodegradable polylactic acid microspheres were prepared using phase inversion nanoencapsulation as previously described [9]. Two formulations were produced: (1) control (no antibody) and (2) purified anti-mouse CD279 (PD-1) antibody (clone J43, BioXCell (West Lebanon, NH), with a loading of 9.25 µg antibody/mg of particles. Control or anti-PD-1 microspheres (0.1 mg particles in 35 µl of sterile water) were administered via intubation-mediated intratracheal instillation (IMIT) two times per week for 4 weeks starting 6 week after adenoviral infection. In some experiments, IL-17A was neutralized by administration of 150 µg of a monoclonal antibody in 0.2 ml saline (clone 17F3, BioXcell) i.p. 3x/week. In other studies γδ T-cells were depleted via i.v. injection of anti- γδ TCR mAb (400 µg, clone UC7-13D5, BioXCell) in 0.2 ml saline (depletion efficacy ≥ 90%). The selective COX-2 inhibitor celecoxib (LC Laboratories, Woburn, MA) was administered (50 mg/kg) starting 6 weeks post-adenoviral infection via oral gavage 5 days per week for 4 weeks.

Preparation of single cell suspensions from the lung

Lung mononuclear cells were isolated as described previously with a modification [9]. Briefly, single-cell suspensions were prepared first by cutting lung into ~1-mm segments, followed with incubation at 37 °C for 30 min in RPMI 1640 in the presence of Liberase TM (50 µg/ml, Roche) and DNase I (1 µg/ml, Thermo Fisher Scientific) with intermittent inversion. Digested lung tissues were then filtered through 70 µm filters into complete RPMI-1640 with 20 mM HEPES, 10% FCS (heat inactivated), 20 mM Glutamine, 1000U/ml Penicillin and 1 mg/ml Streptomycin. A 30:70% (v/v) isotonic discontinuous Percoll (GE Healthcare) density gradient was then used for mononuclear cell enrichment. Cell viability (> 95%) was determined by trypan blue exclusion.

Antibiotic administration and quantification of bacterial burden

To deplete microbiota systemically, mice were given a mix of antibiotics in drinking water containing neomycin (1 g/L), Ampicillin (1 g/L), and Vancomycin (0.5 g/L). Water was changed every 3–4 days. To deplete lung microbiota, mice were given fresh mix of antibiotics containing neomycin (10 g/L), Ampicillin (10 g/L), and Vancomycin (5 g/L) in 35 µl of sterile water via IMIT 2x/week for 4 weeks starting 6 weeks after adenoviral infection. For quantification of bacterial burden, DNA was extracted from all lung tissue samples using the Qiagen DNeasy blood & tissue kit (Qiagen, Valencia, CA, USA). To ensure extraction columns were not overloaded, we used ~ 20 mg of tissue. Nanodrop 2000 (ThermoFisher Scientific) measurements were performed with 2 µL of extracted DNA to determine DNA concentration and purity. The Femto Bacterial DNA Quantification Kit (Zymo Research, Irvine, CA, USA) was used to quantify the extracted bacterial DNA. Each Quantitative PCR (qPCR) sample comprised a 20 µL volume containing 18 µL of Femto Bacterial qPCR premix and 2 µL of either extracted unknown sample DNA, bacterial DNA standard, or no template control. Reactions were run in triplicate and the average calculated starting concentration across all three runs were used as a measure of bacterial load. In studies involving anti-PD-1 treatment, antibiotics were administered via IMIT starting 6 weeks after Ad^{Cre} and 3 days prior to first anti-PD-1 treatment for 4 weeks.

Cytometry by time of flight (CyTOF) analysis and antibody panels

Metal conjugated antibodies were purchased from Fluidigm or were conjugated to unlabeled antibodies in house (Table 1). All non-platinum conjugations were performed using X8 polymer as per manufacturer's protocol (Fluidigm) and were performed at 100 mg or 200 mg scale. Appropriate antibody dilution in the context of each panel was determined by serial dilution staining experiments to minimize background and optimize detection of positively expressing populations. Approximately 2×10^6 lung mononuclear cells were processed for surface and intracellular markers (Helios, Fluidigm) and analyzed using FlowJo software (Tree Star).

Conventional flow cytometry

Fluorescence-conjugated Abs for surface staining, including anti-CD45.2 (104), anti-CD45.1 (A20), anti-CD3 (145-2C11), anti-CD4 (RM4-5), anti-CD8α (53–6.7), anti-CD45R/B220 (RA3-6B2), anti-γδTCR (GL3), anti-CD11b (M1/70), anti-F4/80 (BM8), anti-CX3CR1 (SA011F11), anti–Ly-6C (AL-21), anti–Ly-6G (1A8), anti-Gr1 (RB6-8C5), anti-CD11c (HL3), anti-MHC II (M5/114.15.2), anti-CD140A (APA5), anti-CD326 (EpCAM) (G8.8), anti-CD31 (MEC13.3), anti–IL-17A (TC11-18H10.1), and anti-RORγt (Q31-378) were purchased from BioLegend (San Diego, CA), eBioscience/Thermo Fisher Scientific (Waltham, MA), or BD Biosciences (San Jose, CA). Foxp3 (PJK-16 s; eBioscience) was quantified by intracellular staining performed according to the manufacturer's protocol. To detect the expression of IFNγ and Th17, cells were stimulated for 4–5 h with PMA (Sigma-Aldrich, St. Louis, MO) and ionomycin (Sigma-Aldrich) in the presence of brefeldin A (Sigma-Aldrich) and then stained with anti–IFNγ (XMG1.2) and anti-IL-17A mAb. To detect the expression of IL-1β, IL-23p19, and Cox2, cells were fixed and permeabilized with Foxp3 staining buffers. Cells were then stained with anti-mouse IL-1β (NJTEN3, Invitrogen), anti-mouse IL-23p19 (N71-1183, BD), or anti-mouse Cox2 (EPR18376-119, abcam) at 4 °C for 2 h. A PE-conjugated secondary antibody was followed for detecting Cox2 expression. For CD107a degranulation assay, lung mononuclear cells were cultured in completed RPMI1640 with anti-CD3 (10 µg/ml) and anti-CD28 (1 µg/ml) in 96-well plate for 24 h. Cells were washed and re-stimulated with PMA and ionomycin in the presence of anti-CD107a (1D4B, BioLegend) for additional 4 h. Cells were then stained with antibodies to the appropriate surface receptors. Flow cytometry was performed with BD LSR Fortessa (BD Biosciences) and analysis was performed with FlowJo software (Tree Star).

In vitro $CD4^+$ T-cell priming assay

Naïve $CD3^+CD4^+$ cells were FACS-sorted from lymph nodes of LSL-$Kras^{G12D}$ mice to > 95% purity. Lung interstitial macrophages (IM, $CD11b^{hi}CX3CR1^{hi}CD11c^-CD64^+$) and alveolar macrophages (AM, $CD11b^{low}CX3CR1^-CD11c^{hi}CD64^+$) were sorted from naïve or Ad^{Cre} infected mice with or without antibiotic treatment (oral) 6-weeks post-Ad^{Cre}. $CD4^+$ cells were plated in 96-well plates at a concentration of 1×10^5 cells/0.1 ml RPMI 1640 plus 10% FCS per well. Freshly sorted IM or AM at a concentration of 1×10^4 cells/0.1 ml were added to indicated wells (the ratio of T cell/macrophage is 10:1) for 72 h. $CD4^+$ T cells were then stained for intracellular IL-17A and Foxp3.

Lung COX-2 and PGE_2 quantification

Lung tissues were homogenized with 3.0 mm TriplePure Zirconium beads (Benchmark Scientific, NJ) using a D2400 Homogenizer (setting as 7 m/s, 45 s × 4 cycles with 30 s interval) (Benchmark Scientific, NJ) in 1 ml of T-PER tissue protein extraction reagent containing halt protease inhibitor cocktail (Thermofisher Scientific). Supernatants were collected by centrifugation at 12,000 rpm for 30 min at 4 °C,

Table 1 Summary of antibodies used for CyTOF analysis

Target	Clone	Metal tag	Stain	Dilution	Source	Cat. #
CD45	30-F11	89Y	Surface	150	Fluidigm	3089005B
I-A/I-E	M5/114.15.2	209Bi	Surface	500	Fluidigm	3209006B
NK1.1	PK136	170Er	Surface	150	Fluidigm	3170002B
CD11c	N418	142Nd	Surface	150	Fluidigm	117,341
CD4	RM4-5	145Nd	Surface	150	Fluidigm	3145002B
F4/80	BM8	146Nd	S urface	100	Fluidigm	3146008B
CD3£	145-2C11	152Sm	S urface	150	Fluidigm	3152004B
CD8a	53–6.7	146Nd	S urface	150	Fluidigm	3146003B
CD11 b	M1/70	172Yb	S urface	200	Fluidigm	3172012B
CD64	X54-5/7.1	151Eu	S urface	150	Fluidigm	3151012B
Foxp3	FJK-16 s	158_Gd	intracellular	100	Fluidigm	3158003A
iNOS	CXNFT	161Dy	intracellular	100	Fluidigm	3161011B
RORgt	B2D	159 Tb	intracellular	100	Fluidigm	3159019B
CX3CR1	SA011F11	164Dy	S urface	200	Fluidigm	3164023B
IFNgamma	XMG1.2	165_Ho	intracellular	500	Fluidigm	3165003B
IL-6	MP5-20F3	167_Er	intracellular	100	Fluidigm	3167003B
IL-17A	TC11-18H10.1	174_Yb	i ntracellular	200	Fluidigm	3174002B
CD103	2.00E + 07	148Nd	S urface	150	Biolegend	121,402
TCRgd	GL3	154Sm	S urface	150	Biolegend	118,101
PD-1	29F.1A12	156Gd	S urface	150	Biolegend	109,113
CD107a	1D 4B	169Tm	S urface	300	Biolegend	121,602
IL-12	C15.6	141Pr	intracellular	150	BD	554,477
IL-23p19	N71-1183	176Yb	intracellular	100	BD	565,344
Cox2	Polyclonal	153Eu	intracellular	200	Bio-Rad	AAM13G
Live/Dead	N/A	194Pt/195Pt		1000	Fluidigm	201,194

transferred to clean microcentrifuge tubes and stored at − 80ºC. ELISA kits were used to measure Cox2 (ab210574, abcam) and PGE2 (KGE004B, R&ystems) in according to manufacturer's instructions.

In vitro myeloid cell conditioning and $CD8^+$ T-cell co-culture assays.

FACS sorted IM, AM and monocytes ($CD11b^{hi}Ly\text{-}6C^{hi}$) from LSL-Kras tumor-bearing mice were placed into 24-well plates (1×10^6/ml) in complete RPMI 1640 medium (10% FBS, penicillin/streptomycin, l-glutamine, and sodium pyruvate.). Recombinant murine IL-17A (1 µg/ml) (Peprotech, NJ) was added to indicated wells. The cells were incubated at 37 °C for 5 h and stained intracellularly for COX-2. For co-culture studies, freshly isolated lung mononuclear cells from LSL-Kras tumor-bearing mice were placed in petri dishes for 2 h and adherent cells were harvested as myeloid cells. Myeloid cells were then placed in a 24-well plate (1×10^6/ml) with or without rmIL-17A (1 µg/ml) for 2 h. Concurrent with myeloid cell preparation, $CD8^+$ T cells were positively selected from the spleens of naïve C57BL/6 mouse by magnetic cell sorting using CD8 microbeads (Miltenyi Biotec) per manufacturer's recommendations (average purity of > 95%). $CD8^+$ T cells (1×10^6/ml) were then placed in 96-well U-bottom plates coated with anti-CD3 (5 µg/ml) and anti-CD28 (1 µg/ml). Conditioned myeloid cells were harvested and added to the 96-well plate containing $CD8^+$ T cells (at a T cell/myeloid cell ratio of 2:1) followed by incubation for an additional 24 h. $CD8^+$ T cells were then stained for CD107a.

Statistical analysis

Student's t-test was used to determine the significance of the differences between control and experimental groups in pairwise comparisons. In experiments with multiple groups, homogeneity of intergroup variance was analyzed by one-way ANOVA with multiple pairwise comparisons using Tukey or Holm-Sidak analyses. A p value < 0.05 was considered significant. Each experiment was performed twice, and in some cases three times, to confirm reproducibility.

Results

Th17 Cells are critical to anti-PD-1 resistance

Anti-PD-1 can re-invigorate both pre-existing Th17 and γδ T17 subsets in the dysplastic lungs of LSL-K-ras^{G12D} mice [9]. However, only Th17 (but not γδ T17) cell prevalence correlates with treatment outcome in individual mice suggesting a unique role for the Th17 subset in IL-17-driven anti-PD-1 resistance [9]. To address this conundrum directly, we created a conditional lineage-specific knockout model in which IL-17 production by Th17 cells could be selectively abrogated prior to treatment (Fig. 1A). Specifically, tumors were induced in LSL-K-ras^{G12D} mice that had been engrafted with bone marrow from tamoxifen-inducible CD4^{Cre}RORc $^{fl/fl}$ syngeneic donors, and tamoxifen was administered to delete RORc in CD4$^+$ T-cells starting 5 weeks after tumor induction (Fig. 1B). The mice were then treated with anti-PD-1 for 4 weeks and lung tumor burden was analyzed in control and experimental groups to determine the role of pre-existing Th17 cells in anti-PD-1 resistance (Fig. 1B/C). The data revealed that anti-PD-1 treatment resulted in a 2.5-fold reduction in tumor burden in tamoxifen-treated mice in comparison to control or anti-PD-1-alone groups (Fig. 1C). Importantly, tamoxifen treatment not only resulted in a ~ fourfold reduction in Th17 cell prevalence, but also a concurrent 60% increase in CTL activity (Fig. 1C, Supplemental Fig. 1). The increase in CTL activity was associated with a specific increase in the number of CD107a$^+$ CD8$^+$ T-cells and not with an overall increase in CD8$^+$ T-cell numbers, consistent with activation of pre-existing CTL (Supplemental Fig. 1). These findings confirmed that Th17 cells were the primary mediator of anti-PD-1-induced IL-17 and the associated resistance to therapy in the above model.

Lung microbiota drive the ontogeny of pathogenic Th17 cells

Whereas pro-tumorigenic Th17 cells constitute a significant proportion of lymphocytic infiltrates found in murine and human lung tumors [10], the ontogeny of these cells have not been studied in detail. Gut microbiota has been shown to drive Th17 cell expansion locally in the colon and systemically via the gut-lung axis in lung tumors [11]. Separately, other reports have revealed an important role for local lung microbiome in orchestrating Th17 immunity and tumor growth in the lung [12, 13]. To this end, we examined the potential role of lung microbiota in driving the resident Th17 ontogeny and consequently, anti-PD-1 resistance, in tumor-bearing LSL-Kras^{G12D} mice. To achieve this, we developed an approach that allowed us to selectively deplete lung microbiota via intubation-mediated intratracheal (IMIT) administration of antibiotics. Data shown in Fig. 2A demonstrate that intratracheal antibiotics effectively reduced lung microbial burden while leaving gut microbiota intact.

Next, we undertook an analysis of lung tumor burden and the immune landscape in mice treated with antibiotics to delineate the effects of local microbiota on tumor growth and the associated changes in immune cell subsets. Administration of antibiotics resulted in a twofold decrease in tumor burden in comparison to the control mice, establishing an important role for microbiota in tumor growth (Fig. 2B). Initial global assessment of the lung immune landscape by CyTOF analysis demonstrated that tumor-bearing, microbiota-sufficient mice displayed 2 to 50-fold increases in CD8$^+$ CD103$^+$ T-resident memory cells (Trm), CD4$^+$IFNγ$^+$ Th1 cells, CD4$^+$RORγt$^+$IL-17$^+$ Th17 cells, γδTCR$^+$RORγt$^+$IL-17$^+$ γδT17 cells, CD4$^+$Foxp3$^+$ T-regulatory cells (Treg), CD11b$^+$CD64$^+$CX3CR1$^+$F4/80$^+$ interstitial macrophages (IM) and CD11b^{lo}CD11c$^+$CD64$^+$CX3CR1$^-$F4/80$^+$ alveolar macrophages (AM) in comparison to naïve controls (Fig. 2B). Administration of antibiotics, on the other hand, resulted in a significant abrogation of the increase seen in AM and trended toward partial declines in Th17, γδT17 and Treg, suggesting microbial ontogeny for these subsets (Fig. 2B). In contrast, the prevalence of IFNγ-producing CD8$^+$Trm was enhanced further in the absence of bacteria suggesting a detrimental effect by microbiota on CTL activity.

Targeted analysis of the identified T-cell populations via conventional cytometry essentially confirmed the CyTOF data, i.e., tumor induction resulted in a significant expansion of all CD4$^+$ T-cell subsets in microbiota-sufficient mice with Th17 cells displaying the greatest increase (> fourfold). Treatment with antibiotics, on the other hand, globally abrogated this phenomenon (Fig. 2C). Further quantitative analysis revealed that while microbiota deficiency resulted in an overall decline in total CD4$^+$ T-cell numbers in tumor-bearing mice, there was an additional and significant effect on the Th17 compartment, suggesting that microbiota preferentially drove Th17 ontogeny (Supplemental Fig. 2A).

Importantly, while $CD8^+$ T-cell prevalence data largely replicated the CyTOF findings (not shown), analysis of this subset for membrane CD107a expression revealed that antibiotic treatment resulted in a ~ threefold increase in the percentage of $CD107a^+$ cells (Fig. 2C). Similar to that observed in the $CD4^+$ T-cell-specific RORc knockout mice (Fig. 1C, Supplemental Fig. 1) this increase was primarily associated with cytotoxic activation rather than a general increase in total $CD8^+$ T-cell number (Supplemental Fig. 2B). This observation of increased CTL cytotoxicity co-incident with reduced T17 activity was consistent with the previously-reported ability of IL-17 to suppress antitumor CTL [9].

Analysis of macrophage subsets produced data that partially paralleled CyTOF findings. Specifically, conventional cytometry unmasked an increase in both AM and IM prevalence in tumor-bearing microbiota-sufficient mice in comparison to naïve controls, which returned to near-baseline levels upon antibiotic treatment (Fig. 2D). Importantly, AM and IM isolated from microbiota-sufficient mice displayed increased production of IL-1β and IL-23, suggestive of a phenotype favoring type 17 immunity. Indeed, functional analysis in an in vitro priming assay established that macrophages from microbiota-sufficient mice preferentially polarized $CD4^+$ T-cells toward a Th17 phenotype (Fig. 2D). These data were in line with our previous findings from a separate study, which demonstrated that macrophage depletion in vivo results in dramatic 6 to sevenfold decreases in both Th17 cell prevalence and lung tumor burden in the LSL-$Kras^{G12D}$ model [14]. Collectively, these findings established that macrophages represented a critical link between lung microbiota and Th17 cell activity in the dysplastic lungs of LSL-$Kras^{G12D}$ mice.

We next hypothesized that if microbiota is the primary driver of Th17 cell ontogeny in the dysplastic lung, diminished microbial burden should sensitize LSL-$Kras^{G12D}$ mice to anti-PD-1. To this end, we investigated whether depletion of lung microbiota prior to treatment could improve the efficacy of PD-1 blockade in tumor-bearing mice. The data shown in Fig. 2E demonstrate that while intratracheal antibiotics alone significantly reduced tumor burden, anti-PD-1 treatment resulted in additional, and significant, benefit thus linking the microbiota-macrophage-Th17 cell axis to anti-PD-1 resistance.

IL-17 mediates anti-PD-1 resistance via induction of COX-2/PGE_2

A remaining important question was the nature of the mechanism underlying the ability of Th17 cell-produced IL-17 to interfere with anti-PD-1-mediated CTL re-invigoration. IL-17-dependent recruitment of myeloid-derived suppressor cells (MDSC)/immature neutrophils has been shown to play an important role in IL-17-mediated tumor progression [15–17]. To this end, we first analyzed MDSC prevalence in naïve vs tumor-bearing mice. The data revealed no significant increase in this population in the dysplastic lung (Fig. 3A). To determine whether steady-state MDSC played a role in anti-PD-1 resistance, anti-PD-1 was administered to mice that were depleted of MDSC. Anti-Gr-1 antibody alone or in combination with anti-PD-1 had no significant effect on tumor burden, again suggesting that MDSC did not play a major role in anti-PD-1 resistance in this model (Fig. 3A). In an attempt to demonstrate a link between IL-17 and MDSC infiltration, we performed an additional study in which lung MDSC prevalence was examined in tumor-bearing mice that were treated either by IL-17 neutralizing antibody; anti-PD-1; or both. The data showed no significant changes in MDSC numbers in any of the treatment groups compared to controls (Fig. 3A). Taken together, these data did not support a role for MDSC in IL-17-mediated suppression of anti-PD-1-CTL axis.

IL-17 can promote COX-2 activity and its downstream byproduct PGE_2, a potent inhibitor of T-cell cytotoxic function [18, 19]. To this end, we next investigated a possible role for the IL-17-COX-2/PGE_2 axis in tumor resistance to anti-PD-1 therapy. First, we examined whether neutralization of IL-17 in anti-PD-1-treated mice had any effect on COX-2 or PGE_2 levels in the lung. The data shown in Fig. 3B establish that anti-PD-1 enhanced PGE_2 levels in the lung while neutralization of IL-17 during treatment resulted in a complete abrogation of this effect for both COX-2 and PGE_2. We then asked whether COX-2 was responsible for de-sensitization of tumors to anti-PD-1 treatment. Inhibition of COX-2 activity resulted in significant enhancement of tumor suppression in anti-PD-1 treated mice (Fig. 3C). Moreover, while COX-2 inhibition did not alter Th17 activity, it enhanced cytotoxic function of CTL by 60% in the lungs of tumor-bearing mice (Fig. 3C). Again, this increase was primarily due to activation of pre-existing CD8 + T-cells and not to a broad increase in $CD8^+$ T-cell numbers (Supplemental Fig. 3A). In addition, COX-2 inhibition did not alter overall $CD4^+$ T-cell, Th1 or Treg numbers, ruling out secondary effects involving $CD4^+$ T-cells (Supplemental Fig. 3). Collectively, these data supported a major role for the anti-PD-1-IL-17-COX-2/PGE_2 axis in de-sensitization of CTL and tumors to anti-PD-1 treatment.

COX-2 can be expressed by different cell types in inflammatory microenvironments [20]. A global screening approach was employed next to identify the primary cellular source of COX-2 in the lungs of anti-PD-1 treated animals. Specifically, intracellular staining of $CD45^+$ cells revealed that anti-PD-1 treatment induced significant COX-2 in cells of myeloid origin including IM, AM, $CD11b^+Ly6C^+Ly6G^-CD64^-$ monocytes (Mono) and $CD11c^+MHCII^+CD64^-$ dendritic cells (DC) (Fig. 3D). $CD3^+$ T-cells also displayed a statistically-significant, but more

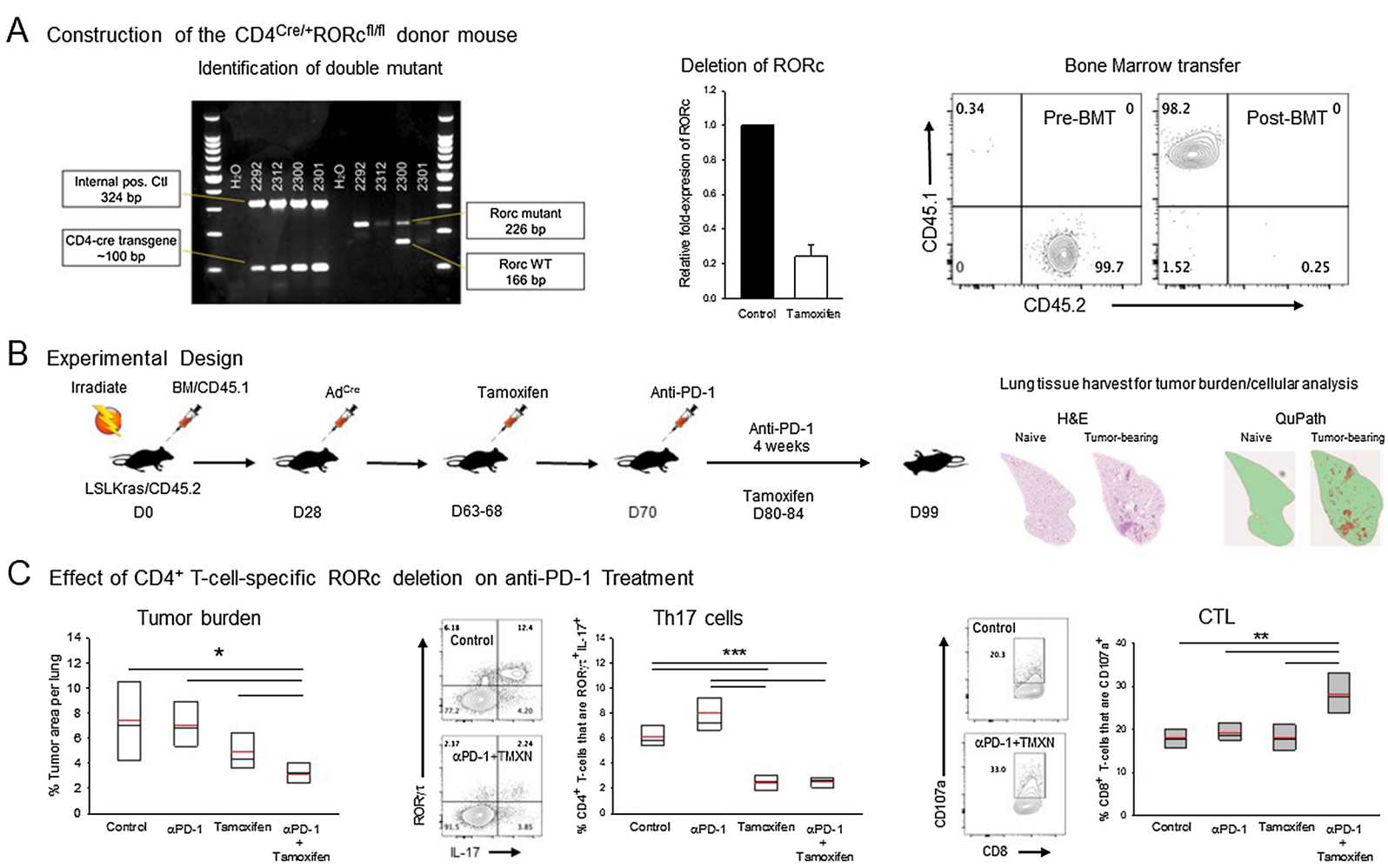

Fig. 1 Construction of the LSL-Kras^{G12D} bone marrow chimeric mouse and effect of RORc ablation on anti-PD-1 treatment. *Panel A*. Creation of the bone marrow chimera. C57Bl6 RORc$^{fl/fl}$ mice were backcrossed into tamoxifen-inducible CD4^{Cre} background creating the CD45.1^{+}CD4$^{Cre/+}$RORc$^{fl/fl}$ donor strain. An agarose gel marker analysis of the backcrossed mice is shown in which mouse 2292 depicts the double mutant (left panel). The efficacy of tamoxifen-induced ablation of RORc in CD4^{+} cells was then tested in the double-mutant (middle panel). Relative-fold expression of RORc in CD4^{+} cells purified from control vs tamoxifen-treated mice was determined by qPCR (Error bars = S.E.M., n = 3). Efficacy of bone marrow transfer was determined by analysis of CD4^{+} T-cells in sera obtained from CD45.2^{+} LSL-K-ras^{G12D} recipients prior to (pre-BMT) or 4 weeks after engraftment (post-BMT) of CD45.1^{+} donor bone marrow (right panel). *Panel B*. Experimental design for tamoxifen-induced RORc ablation in tumor-bearing bone-marrow engrafted LSL-K-ras^{G12D} mice followed by anti-PD-1 treatment. Examples of H&E stained lung sections and quantitative QuPath images of these sections are shown (red depicts tumor area). *Panel C*. Effect of CD4^{+} T-cell-specific RORc deletion on tumor burden and T-cell phenotype/function. Tumor burden, Th17 cell and CD8.$^{+}$ cytotoxic T-lymphocyte (CTL) prevalence were determined in control (untreated) and experimental mice. Boxes have lines at the median (black) and mean (red) showing lower (25%) and upper (75%) quartiles (n = 5 per group, *,**,*** depict $p < 0.05, 0.01, 0.001$, respectively)

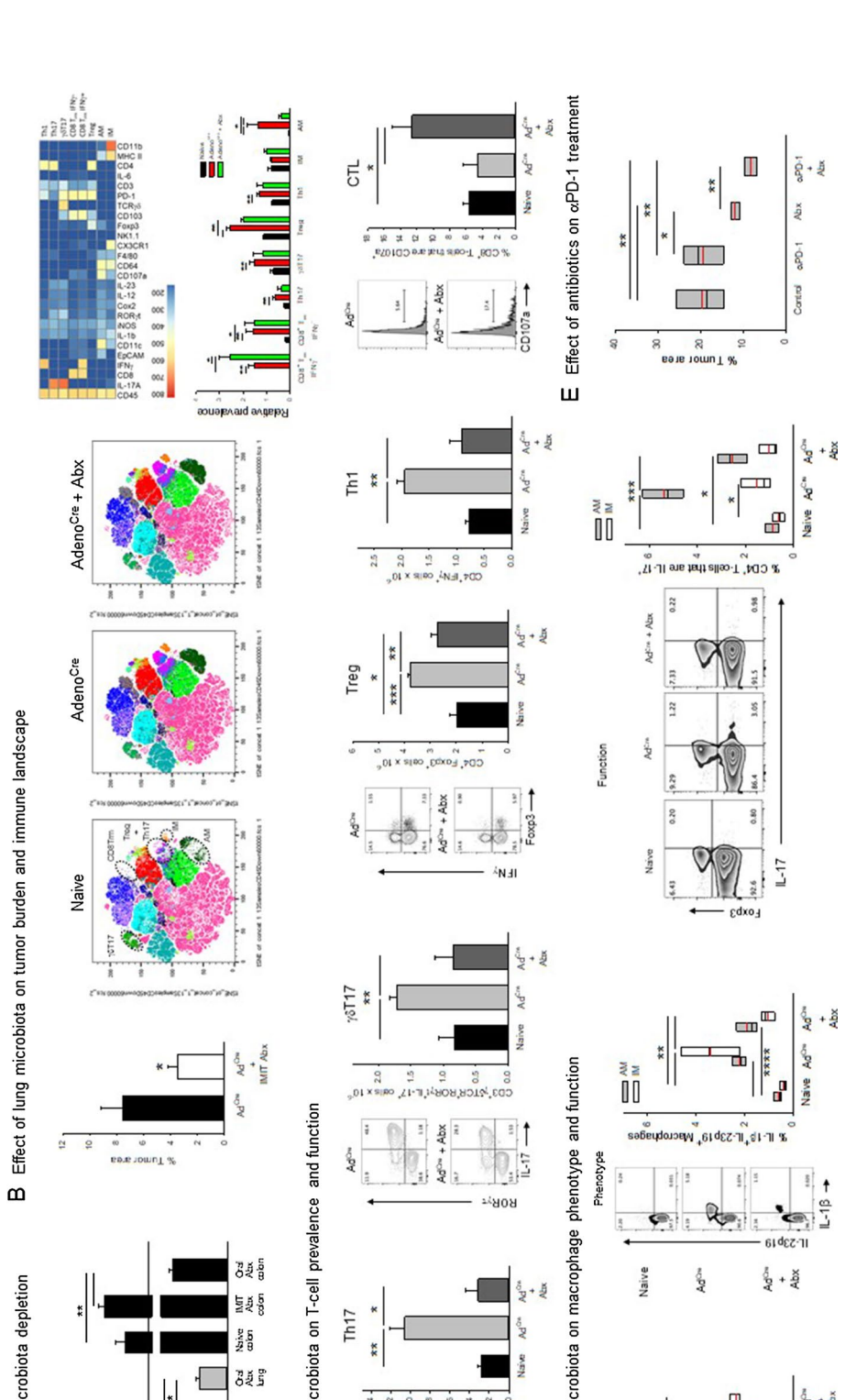

Fig. 2 Effect of lung microbiota on tumor burden, immune landscape and anti-PD-1 treatment. *Panel A*. Efficacy and specificity of lung microbiota depletion. Mice were either treated with oral or intratracheal (via IMIT) antibiotics and lung as well as colon bacterial burden were compared to naïve controls. Relative bacterial burden (to kit standard) for each group is shown. Error bars = S.E.M. (n = 3–8 mice per group). *Panel B*. Effect of antibiotic treatment on tumor growth and lung immune landscape. Tumors were induced in control vs antibiotic-treated (via IMIT) mice followed by analysis of tumor burden and immune cell populations. Of the 24 clusters that were identified by CyTOF analysis, those that demonstrated major changes in tumor-bearing vs naïve animals are shown (dotted line circles). A representative heat map for the markers used to identify the selected clusters and quantitative analyses of these subsets are also presented. Error bars = S.E.M. (n = 7–8 per group for tumor burden and 3–5 per group for CyTOF analysis). *Panel C*. Effect of antibiotics on T-cell subset prevalence and function as assessed by conventional flow cytometry. Single cell suspensions prepared from lungs were analyzed for the indicated subsets/markers for prevalence and function. Specifically, $CD3^+CD4^+$ T-cells were gated on and analyzed for the indicated Th1, Th17 and Treg markers; $CD3^+\gamma\delta TCR^+$ cells were gated on and analyzed for RORγt and IL-17 (γδT17 cells); $CD3^+CD8^+$ cells were gated on and analyzed for CD107a (CTL). Error bars = S.E.M. (n = 3–5 per group). *Panel D*. Effect of antibiotics on macrophage subsets in the lung. IM and AM were analyzed for prevalence (numbers per lung); for phenotype (by cytokine secretion); and for function (ability to induce IL-17 in $CD4^+$ T-cells). Sample flow panels (AM) and quantitative data are shown. Boxes have lines at the median (black) and mean (red) showing lower (25%) and upper (75%) quartiles (n = 5 per group). Panel E. Effect of antibiotic administration on efficacy of anti-PD-1 treatment. Tumor-bearing mice were treated either with anti-PD-1 alone, antibiotics alone or a combination. Control mice received vehicle. Boxes have lines at the median (black) and mean (red) showing lower (25%) and upper (75%) quartiles (n = 5 per group). Significance: *, **, ***, **** depict $p < 0.05$, 0.01, 0.001, 0.0001, respectively

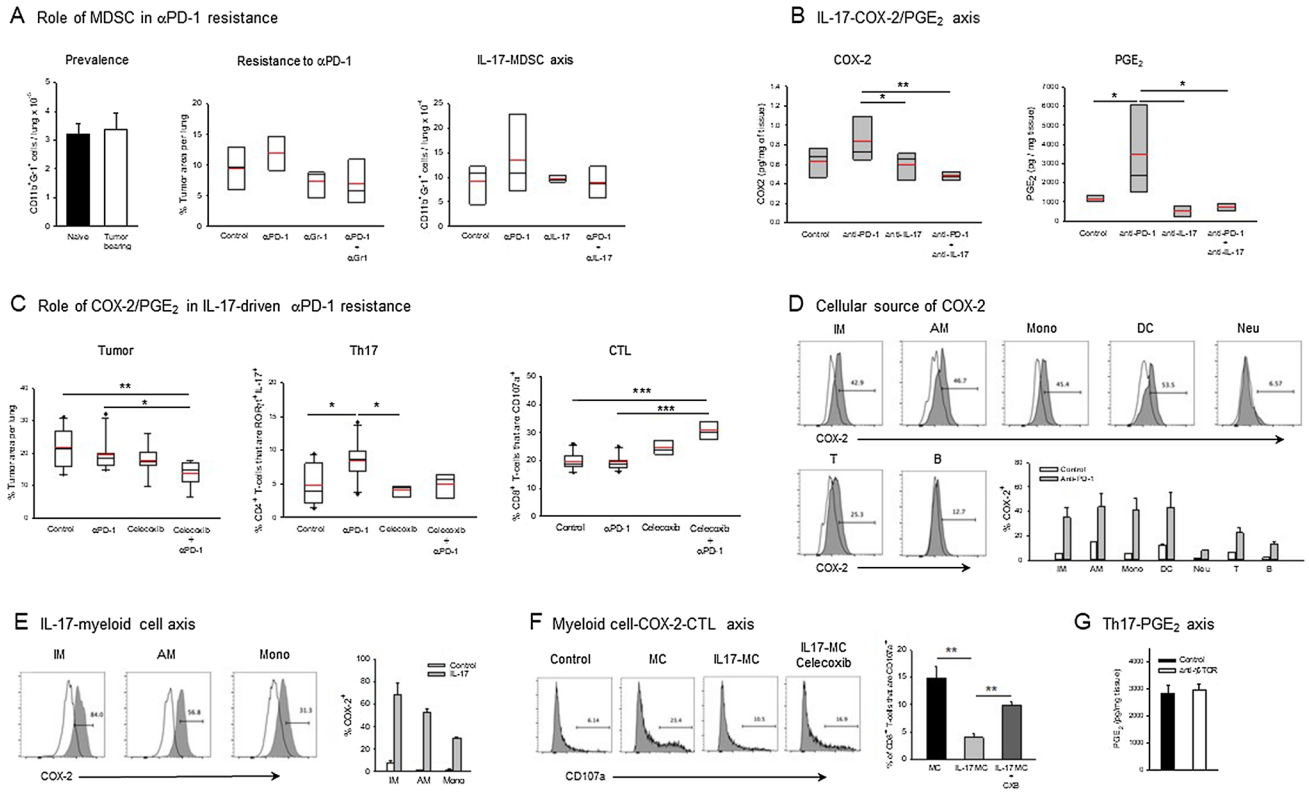

Fig. 3 Mechanism of IL-17-driven anti-PD-1 resistance. *Panel A*. Role of MDSC. Prevalence of MDSC in the lung was determined in age-matched naïve vs tumor-bearing (10 weeks post-Ad^{Cre}) mice. Error bars = S.E.M. (n = 9–11 per group). Resistance to anti-PD-1 was determined in control vs MDSC-depleted (anti-Gr-1) mice. Mice were administered anti-Gr-1 antibody (200 μg anti-Gr-1 antibody in 0.2 ml, i.p. 3×per week) starting 6 weeks post-Ad^{Cre} and 3 days prior to first anti-PD-1 treatment. Lungs were analyzed for tumor burden after 4 weeks of treatment. Controls received vehicle (n = 4 per group). The effect of IL-17 neutralization on MDSC prevalence during anti-PD-1 treatment (anti-IL-17 antibody administered starting 6 weeks post-Ad^{Cre} and 3 days prior to first anti-PD-1 treatment) was evaluated (right panel, n = 4 per group). Control mice received vehicle. Boxes have lines at the median (black) and mean (red) showing lower (25%) and upper (75%) quartiles. No significant differences were observed between any of the groups. *Panel B*. Effect of anti-PD-1 and IL-17 on lung COX-2/PGE_2 levels. Lung COX-2 and PGE_2 levels were determined in mice treated with anti-PD-1 in the absence or presence of IL-17 neutralization. Control mice received vehicle. Boxes have lines at the median (black) and mean (red) showing lower (25%) and upper (75%) quartiles (n = 5 per group). *Panel C*. Effect of COX-2 inhibition on treatment and T-cell immunity. Tumor-bearing mice were treated with anti-PD-1 in the presence or absence of a COX-2 inhibitor (celecoxib) and lung tumor burden as well as Th17 cell prevalence and CTL function were evaluated (n = 8–11 per group). Boxes have lines at the median (black) and mean (red) showing lower (25%) and upper (75%) quartiles. Whiskers extend to show the 10^{th} and 90^{th} percentiles with symbols representing the extreme values (in groups with n ≥ 9). Panel D. Cellular source of COX-2. Single cell suspensions prepared from tumor-bearing control or anti-PD-1-treated mice were analyzed for intracellular COX-2. Representative histograms and quantitative data are shown for immune cell subsets (control untreated [open histograms/bars] and anti-PD-1-treated [filled histograms/bars]). Error bars = S.E.M. (n = 3 per group, $p < 0.05$ control vs anti-PD-1 for all subsets except B cells). Panel E. IL-17 stimulation of myeloid cells. Representative histograms and quantitative data are shown for control (myeloid cell subsets alone, open histograms/bars) and IL-17-conditioned myeloid cell subsets (filled histograms/bars) stained for COX-2 expression. Error bars = S.E.M., n = 3 per group. Panel F. Effect of myeloid cell conditioning with IL-17 on CTL activity. Representative histograms and quantitative data are shown for $CD8^+$ T-cell CD107a expression in control ($CD8^+$ T-cells alone) and experimental groups ($CD8^+$ T-cells co-cultured with myeloid cells [MC]; IL-17-conditioned MC or IL-17-conditioned MC in the presence of celecoxib [CXB]). Quantitative data shown are with control value subtracted as background. Error bars = S.E.M., n = 4 per group. Panel G. Lung PGE_2 levels in post-anti-PD-1 mice. Lung PGE_2 levels were determined in anti-PD-1-treated mice in the absence (control) or presence of γδ T-cell depletion (anti-γδ TCR). For this study, tumor-bearing mice were injected either with vehicle or anti-γδ TCR antibody and were treated with anti-PD-1 24 h later. Lungs were harvested and analyzed 24 h after anti-PD-1 treatment. Error bars = S.E.M., n = 4 and 11 for control and anti-gdTCR groups, respectively. Significance: *, **, *** depict $p < 0.05$, 0.01, 0.001, respectively, for all panels

modest overall increase whereas $CD11b^+Ly6G^+Ly6C^-$ neutrophils and $B220^+$ B-cells were not major sources. In contrast, stromal cells ($CD45^-CD140A^+$ fibroblasts, $CD45^-EpCAM^+$ epithelial cells and $CD45^-CD31^+$ endothelial cells) did not display any detectable increase in COX-2 expression in treated animals (data not shown).

To determine whether IL-17 directly induced COX-2 expression in myeloid cells; AM, IM and monocytes sorted from tumor-bearing lungs were cultured with recombinant murine IL-17. The results revealed significant 10 to 35-fold increases in COX-2 expression in IL-17-conditioned myeloid cell subsets compared to controls (Fig. 3E). Importantly, IL-17-conditioned myeloid cells displayed reduced ability to induce $CD8^+$ T-cell cytotoxicity in vitro, but this was reversed in the presence of celecoxib further confirming the direct role of myeloid-cell derived COX-2/PGE_2 in suppressing CTL function (Fig. 3F). Finally, anti-PD-1 treatment induced similar levels of COX-2 (Supplemental Fig. 4) and PGE_2 (Fig. 3G) in γδ T-cell deficient vs sufficient mice, confirming that COX-2/PGE_2 expression was primarily driven by Th17 cell-produced IL-17.

Discussion

This study provides new mechanistic insight into a recently identified paradigm in anti-PD-1 resistance [9]. Specifically, our data establish that activation of the pre-existing Th17 cells by anti-PD-1 antibody is the primary driver of ICB resistance in the LSL-K-ras^{G12D} model; that the ontogeny of these cells, and thus tumor resistance, is driven by lung microbiota-conditioned macrophages; and that the effector mechanism involves the IL-17-COX-2/PGE_2 axis. These findings have important clinical implications as both IL-17-neutralizing antibodies and COX-2 inhibitors are readily available in the clinic.

Whereas anti-PD-1 can re-invigorate both lung-resident Th17 and γδT17 cells in the above model, therapeutic outcome correlates with Th17-, but not with γδT17-cell, prevalence in post-treatment mice [9]. The data from the genetic model, in which targeted ablation of RORc in $CD4^+$ T-cells resulted in the reversal of anti-PD-1 resistance, confirm the primary role of Th17 cells in mediating the therapeutic effect. One potential explanation for the unique role of Th17 subset in this setting likely involves the pre-therapy functional state of the two subsets. Specifically, our studies indicate that at steady-state γδT17 cells produce IL-17 constitutively independent of PD-1 blockade, which is enhanced only by ~ 40% upon PD-1 blockade [9]. In contrast, Th17 cells display a quiescent phenotype at steady-state but exhibit a threefold increase in % $IL\text{-}17^+$ cells upon exposure to anti-PD-1 [9]. Given this information, as well as the lack of significant changes in total $CD4^+$ T-cell, Th1 or Treg subset prevalence in anti-PD-1-treated mice, we propose that while γδT-cells may be the primary producers of IL-17 at steady-state, re-invigorated Th17 cells provide the bulk of IL-17 in post-anti-PD-1 mice and therefore are the primary drivers of anti-PD-1 resistance.

The requirement for lung microbiota in driving the ontogeny of resident Th17 cells and tumor resistance to anti-PD-1, and the central role of macrophages in mediating this process, is consistent with our previous report on the ability of IL-10 to disrupt the pro-tumorigenic macrophage-Th17 axis in the lung [14]. Our data also recapitulate and extend the findings in the double-mutant KP model in which the authors demonstrated a link between lung microbiota, IL-1β/IL-23-producing myeloid cells and γδT17 cell expansion [17]. Herein, we did not attempt to identify the specific bacterial species that drive this process or the underlying molecular mechanism. Several studies have demonstrated that in the human distinct bacterial species are associated with type 17 immunity and tumor progression in the lung [12, 13]. In addition, a recent report revealed a critical role for bacterial peptidoglycans in modulating the response to ICB [21]. Whether similar genera/species and/or mechanisms drive the pathogenic Th17 cell activity in the LSL-$Kras^{G12D}$ mice remains to be determined.

Studies in murine lung cancer models have identified a strong link between IL-17, its ability to recruit MDSC/suppressive neutrophils and enhance tumor growth/resistance to immune therapy [15–17]. In contrast, our data do not support a major role for MDSC in IL-17-mediated anti-PD-1 resistance. One possible explanation for this seeming contradiction may involve the degree of tumor burden at the time of treatment, which can influence MDSC generation/recruitment. For example, in a previous study in which authors demonstrated a strong link between IL-17 and MDSC in LSL-K-ras^{G12D} mice, analyses were performed in mice with advanced disease (22 weeks after tumor induction) [15]. Similarly, in the more aggressive KP model, a link between IL-17 and neutrophil infiltration was demonstrated at 15 weeks post-tumor induction [17]. In contrast, we analyzed tumor burden 10 weeks after Ad^{Cre} administration. Therefore, we expect that IL-17 driven tumor growth and/or resistance to anti-PD-1 can be mediated by multiple non-mutually-exclusive mechanisms in a tumor phenotype/stage/burden-dependent manner.

The above findings are consistent with the broad literature demonstrating a pathogenic role for IL-17 in NSCLC [22]. Based on these reports a potential synergy between IL-17 blockade and anti-PD-1 therapy has been proposed, but has not yet been tested in the clinic [23]. Our findings support the utility of such a combinatorial strategy as an active treatment modality designed to abrogate the pro-tumorigenic effects of PD-1 blockade on Th17 immunity. In addition, identification of the IL-17-COX-2 link opens

up the possibility of using orally-available COX-2 inhibitors in combination with anti-PD-1, providing a more clinically feasible approach.

Supplementary Information The online version contains supplementary material available at https://doi.org/10.1007/s00262-022-03285-3.

Author contributions NKE: Original concept, design and supervision of studies, data interpretation, manuscript preparation, funding. QL: Study design, execution of experiments, data interpretation, manuscript preparation. KEG and SYS: technical help with experiments. JMW: IMIT administration and technical training.

Funding This work was supported by the Department of Defense Lung Cancer Research Program Idea award W81XWH1910265 (NKE) and in part by the NIH NIGMS CoBRE award P20-GM135004 (QL).

Availability of data and material All data will be made available upon request.

Code availability Non applicable.

Declarations

Conflict of interests N.K.E has ownership interest in Therapyx, Inc. The remaining authors declare no competing financial interests.

Ethics approval Animal studies were approved by the University of Louisville IACUC.

Consent to participate All authors consented to participate in these studies.

Consent for publication All authors consent to publication of the findings.

References

1. Reck M, Remon J, Hellmann MD (2022) First-line immunotherapy for non-small-cell lung cancer. J Clin Oncol 40:586–597. https://doi.org/10.1200/JCO.21.01497
2. Tunger A, Sommer U, Wehner R et al (2019) The evolving landscape of biomarkers for anti-PD-1 or anti-PD-L1 therapy. J Clin Med. https://doi.org/10.3390/jcm8101534
3. Laba S, Mallett G, Amarnath S (2021) The depths of PD-1 function within the tumor microenvironment beyond CD8(+) T cells. Semin Cancer Biol. https://doi.org/10.1016/j.semcancer.2021.05.022
4. Francisco LM, Salinas VH, Brown KE, Vanguri VK, Freeman GJ, Kuchroo VK, Sharpe AH (2009) PD-L1 regulates the development, maintenance, and function of induced regulatory T cells. J Exp Med 206:3015–3029. https://doi.org/10.1084/jem.20090847
5. Franceschini D, Paroli M, Francavilla V, Videtta M, Morrone S, Labbadia G, Cerino A, Mondelli MU, Barnaba V (2009) PD-L1 negatively regulates CD4+CD25+Foxp3+ Tregs by limiting STAT-5 phosphorylation in patients chronically infected with HCV. J Clin Invest 119:551–564. https://doi.org/10.1172/JCI36604
6. Tan CL, Kuchroo JR, Sage PT et al (2021) PD-1 restraint of regulatory T cell suppressive activity is critical for immune tolerance. J Exp Med. https://doi.org/10.1084/jem.20182232
7. Kamada T, Togashi Y, Tay C et al (2019) PD-1(+) regulatory T cells amplified by PD-1 blockade promote hyperprogression of cancer. Proc Natl Acad Sci U S A 116:9999–10008. https://doi.org/10.1073/pnas.1822001116
8. Balanca CC, Salvioni A, Scarlata CM et al (2021) PD-1 blockade restores helper activity of tumor-infiltrating, exhausted PD-1hiCD39+ CD4 T cells. JCI Insight. https://doi.org/10.1172/jci.insight.142513
9. Li Q, Ngo PT, Egilmez NK (2021) Anti-PD-1 antibody-mediated activation of type 17 T-cells undermines checkpoint blockade therapy. Cancer Immunol Immunother 70:1789–1796. https://doi.org/10.1007/s00262-020-02795-2
10. Kuen DS, Kim BS, Chung Y (2020) IL-17-Producing cells in tumor immunity: friends or foes? Immune Netw 20:e6. https://doi.org/10.4110/in.2020.20.e6
11. Bradley CP, Teng F, Felix KM et al (2017) Segmented filamentous bacteria provoke lung autoimmunity by inducing gut-lung axis Th17 cells expressing dual TCRs. Cell Host Microbe 22(697–704):e4. https://doi.org/10.1016/j.chom.2017.10.007
12. Segal LN, Clemente JC, Tsay JC et al (2016) Enrichment of the lung microbiome with oral taxa is associated with lung inflammation of a Th17 phenotype. Nat Microbiol 1:16031. https://doi.org/10.1038/nmicrobiol.2016.31
13. Tsay JJ, Wu BG, Sulaiman I et al (2021) Lower airway dysbiosis affects lung cancer progression. Cancer Discov 11:293–307. https://doi.org/10.1158/2159-8290.CD-20-0263
14. Li Q, Anderson CD, Egilmez NK (2018) Inhaled IL-10 suppresses lung tumorigenesis via abrogation of inflammatory macrophage-Th17 cell axis. J Immunol 201:2842–2850. https://doi.org/10.4049/jimmunol.1800141
15. Chang SH, Mirabolfathinejad SG, Katta H, Cumpian AM, Gong L, Caetano MS, Moghaddam SJ, Dong C (2014) T helper 17 cells play a critical pathogenic role in lung cancer. Proc Natl Acad Sci U S A 111:5664–5669. https://doi.org/10.1073/pnas.1319051111
16. Akbay EA, Koyama S, Liu Y et al (2017) Interleukin-17A promotes lung tumor progression through neutrophil attraction to tumor sites and mediating resistance to PD-1 blockade. J Thorac Oncol 12:1268–1279. https://doi.org/10.1016/j.jtho.2017.04.017
17. Jin C, Lagoudas GK, Zhao C et al (2019) Commensal microbiota promote lung cancer development via gammadelta T cells. Cell 176(998–1013):e16. https://doi.org/10.1016/j.cell.2018.12.040
18. Li Q, Liu L, Zhang Q, Liu S, Ge D, You Z (2014) Interleukin-17 Indirectly Promotes M2 Macrophage Differentiation through Stimulation of COX-2/PGE2 Pathway in the Cancer Cells. Cancer Res Treat 46:297–306. https://doi.org/10.4143/crt.2014.46.3.297
19. Basingab FS, Ahmadi M, Morgan DJ (2016) IFNgamma-dependent interactions between ICAM-1 and LFA-1 counteract prostaglandin E2-mediated inhibition of antitumor CTL responses. Cancer Immunol Res 4:400–411. https://doi.org/10.1158/2326-6066.CIR-15-0146
20. Gomez-Valenzuela F, Escobar E, Perez-Tomas R, Montecinos VP (2021) The inflammatory profile of the tumor microenvironment, orchestrated by cyclooxygenase-2. Promotes Epithel-Mesenchymal Trans Front Oncol 11:686792. https://doi.org/10.3389/fonc.2021.686792
21. Griffin ME, Espinosa J, Becker JL, Luo JD, Carroll TS, Jha JK, Fanger GR, Hang HC (2021) Enterococcus peptidoglycan remodeling promotes checkpoint inhibitor cancer

immunotherapy. Science 373:1040–1046. https://doi.org/10.1126/science.abc9113
22. Joerger M, Finn SP, Cuffe S, Byrne AT, Gray SG (2016) The IL-17-Th1/Th17 pathway: an attractive target for lung cancer therapy? Expert Opin Ther Targets 20:1339–1356. https://doi.org/10.1080/14728222.2016.1206891
23. Nagaoka K, Shirai M, Taniguchi K et al (2020) Deep immunophenotyping at the single-cell level identifies a combination of anti-IL-17 and checkpoint blockade as an effective treatment in a preclinical model of data-guided personalized immunotherapy. J Immunother Cancer. https://doi.org/10.1136/jitc-2020-001358